INFORMATION TO USERS

This was produced from a copy of a document sent to us for microfilming. While the most advanced technological means to photograph and reproduce this document have been used, the quality is heavily dependent upon the quality of the material submitted.

The following explanation of techniques is provided to help you understand markings or notations which may appear on this reproduction.

1. The sign or "target" for pages apparently lacking from the document photographed is "Missing Page(s)". If it was possible to obtain the missing page(s) or section, they are spliced into the film along with adjacent pages. This may have necessitated cutting through an image and duplicating adjacent pages to assure you of complete continuity.

2. When an image on the film is obliterated with a round black mark it is an indication that the film inspector noticed either blurred copy because of movement during exposure, or duplicate copy. Unless we meant to delete copyrighted materials that should not have been filmed, you will find a good image of the page in the adjacent frame.

3. When a map, drawing or chart, etc., is part of the material being photographed the photographer has followed a definite method in "sectioning" the material. It is customary to begin filming at the upper left hand corner of a large sheet and to continue from left to right in equal sections with small overlaps. If necessary, sectioning is continued again—beginning below the first row and continuing on until complete.

4. For any illustrations that cannot be reproduced satisfactorily by xerography, photographic prints can be purchased at additional cost and tipped into your xerographic copy. Requests can be made to our Dissertations Customer Services Department.

5. Some pages in any document may have indistinct print. In all cases we have filmed the best available copy.

University
Microfilms
International

300 N. ZEEB ROAD, ANN ARBOR, MI 48106
18 BEDFORD ROW, LONDON WC1R 4EJ, ENGLAND

TAYLOR, ROBERT EDWARD

PROTON NMR OF HYDROGEN(1.7) MOLYBDENUM-TRIOXIDE AND YTTYIUM-HYDROGEN(1.92)

Iowa State University PH.D. 1980

Proton NMR of $H_{1.7}MoO_3$ and $YH_{1.92}$

by

Robert Edward Taylor

A Dissertation Submitted to the

Graduate Faculty in Partial Fulfillment of the

Requirements for the Degree of

DOCTOR OF PHILOSOPHY

Department: Chemistry
Major: Physical Chemistry

Approved:

Signature was redacted for privacy.

In Charge of Major Work

Signature was redacted for privacy.

For the Major Department

Signature was redacted for privacy.

For the Graduate College

Iowa State University
Ames, Iowa

1980

TABLE OF CONTENTS

LIST OF FIGURES

LIST OF TABLES

INTRODUCTION

There has been a recent surge in the applications of nuclear magnetic resonance (NMR) spectroscopy, particularly in solids, to the solution of a wide variety of problems of very practical natures. These have included the investigations of spatially controlled NMR techniques as a diagnostic tool for cancer (1-4) as well as the more typical applications in the studies of catalysts (5, 6), polymers (7-9), fossil fuels (10), and metal hydrides (11). The sensitivity of NMR to the local environment on an atomic scale for a particular nucleus provides information about electronic structure as well as molecular structure and motion.

NMR spectroscopy provides this information through the perturbation of nuclear spin states. The total nuclear spin Hamiltonian is a sum of Hamiltonians describing the physically different interactions of the nuclear spins. For example, these include the nuclear dipole interaction, nuclear quadrupole coupling, Knight shift coupling, and hyperfine coupling. Generally, serveral interactions contribute simultaneously to the relaxation of the nuclear spin system in an NMR experiment. Although each of these interactions contains useful information, the NMR spectrum usually can be interpreted to give only the largest one or complex combination of a couple. The use of recentiy developed NMR techniques (12, 13) allows the separation and characterization of the interactions present.

In particular, the work described in this thesis deals with the application of a variety of existing time dependent techniques in NMR as well as the extension of high resolution techniques and their use to learn more about the nature and mobility of protons in $H_{1.7}MoO_3$ and $YH_{1.92}$. The reasons for the choice of these particular chemical systems are two fold. The physical properties of these systems are particularly well-suited to be studied by solid state NMR. Secondly, they are of practical importance. The compound $H_{1.7}MoO_3$ has been proposed (14) to be a model system for providing information about the reduction of supported molybdenum oxide catalysts. Metal hydrides, such as $YH_{1.92}$, have possible technological applications for hydrogen storage.

LITERATURE REVIEW

Since this dissertation deals both with the extension of high resolution experiments in solid state NMR and with the application of these techniques as well as existing methods to chemical systems, this literature review is informally divided into three sections. The first presents a brief review of the history of NMR and the use of time dependent experiments in NMR to selectively average specific interactions. The latter two sections introduce the chemical systems and specific goals for this research.

Much of the research effort in the years immediately following the discovery of NMR in 1945 by Bloch et al. (15) and Purcell et al. (16) was aimed at understanding the response of the nuclear spin system to applied magnetic fields as well as those within the matter containing the spin system. Some of the classic papers during this period dealt with spin relaxation (Bloembergen, Purcell, and Pound (17)), the discovery of the chemical shift by Proctor and Yu (18), the theoretical formulation of the chemical shift by Ramsey (19), and the extension of nuclear spin relaxation theory to translational diffusion by Torrey (20). One of the most important papers, not only in terms of theory but also from a technological point of view, was the demonstration by Lowe and Norberg (21) that the steady state resonance condition in the frequency domain was the Fourier transform of the free induction decay in the time domain. In the years that followed, NMR was

considered to be a mature research method and the emphasis was placed on the applications of existent experiments to an understanding of physical and chemical processes. The research situation at that time is probably best described by Mehring et al. (22).

> "The early era of the chemical shift provided the experimental practitioner of NMR not only with a challenge in technique but also with the dual rewards of (a) relevance to the problems of chemical society and (b) an opportunity to confound the dogmas of valence theory. History relates that the technical challenges were quickly met, the theorists showed their customary adaptability to experimental fact, and the chemical shift relaxed into the embrace of the capitalist and the analytical chemist."

As discussed in the Introduction, several interactions contribute simultaneously to the relaxation of the nuclear spin system in a NMR experiment. In general, these lead to broad featureless absorption lines, devoid of much chemically interesting information. For example, the nuclear dipolar interaction may be several orders of magnitude larger than the entire range of isotropic chemical shifts for a given nucleus. The experimental access to information such as chemical shifts, when obscured by much larger interactions, relies on motional averaging. The best example is the narrow NMR lines observed in solution due to the rapid, random, isotropic reorientational and translational motions of molecules in liquids. In solution, the dipolar interactions are averaged to zero. However, all information concerning the anisotropic interactions of the spins is also lost. Since anisotropic spin interactions can be obtained only from solids, other methods of averaging interactions were developed.

The first attempts to selectively remove interactions were made by E. R. Andrew et al. (23-29) and I. Lowe (30) in the late fifties and early sixties. The technique of high speed sample rotation modulates the real space (as opposed to the spin space) portion of the nuclear dipolar interaction (31) given by $(1 - 3\cos^2\theta_{ij})r_{ij}^{-3}$, where θ_{ij} is the angle between the internuclear spin vector, $\vec{r}_{ij}$, and the external magnetic field, by introducing a time dependence into θ_{ij}. As a result, if the sample is rotated with a uniform angular velocity larger than the natural linewidth about an axis inclined at an angle α with respect to the external magnetic field, the dipolar interaction is time averaged and is attenuated by the factor $\frac{1}{2}(3\cos^2\alpha - 1)$. If the axis of rotation is inclined at an angle of arc cos $(\frac{1}{\sqrt{3}})$, the magic angle, the dipolar interaction is effectively zero. However, E. R. Andrew et al. (32, 33) and I. Lowe (30) realized that the second rank tensor describing the magnetic shielding also has a factor $\frac{1}{2}(3\cos^2\alpha - 1)$ introduced by high speed sample rotation. At the magic angle, where the dipolar broadening is suppressed, only the trace of the shielding tensor is obtained. While this quantity does provide information about molecular structure, all anisotropic information, once again, is lost.

In 1968, the research groups of P. Mansfield and of J. S. Waugh (34-38, 44, 45) demonstrated the interactions could be selectively removed from the description of the spin system by

showing that "motional averaging" can also occur in spin space with properly chosen radiofrequency fields. By manipulating the time development of the nuclear spin system with a cycle of intense (r.f. field much larger than local dipolar fields) radiofrequency pulses, the time evolution of the spin system can be described by an "average" Hamiltonian (39). If the pulse sequence is judiciously chosen to meet certain periodic and cyclic conditions (35), the homonuclear dipolar interaction can be severly attenuated. The real beauty of this multiple pulse technique is that while the homonuclear dipolar broadening is suppressed, the information concerning anisotropic spin interactions is still retained (22).

This pioneering work has led to a resurgence in investigations of the response of the nuclear spin system to various applied radiofrequency pulse sequences. Specifically, W.-K. Rhim et al. (40-43) and P. Mansfield (44, 45) have developed improved mutliple pulse sequences to better handle errors and non-idealities in the pulses as well as higher order dipolar terms in the average Hamiltonian. By introducing deliberate errors into one of the radiofrequency phases of the multiple pulse sequence, Vaughan et al. (46, 47) were able to further separate the contributions to the linewidth from static magnetic field inhomogeneity (which includes shielding anisotropies), higher order dipolar broadening, and lifetime broadening under the multiple pulse sequence. Dybowski

and Pembleton (48) developed a dipolar narrowed version of the Carr-Purcell (49) sequence, which was designed to remove the need for the introduction of a phase error in order to measure the lifetime broadening under multiple pulse sequences.

Even with the ability to suppress dipolar broadening with multiple pulse homonuclear decoupling techniques or with the simpler heteronuclear decoupling (50, 51) techniques, it is still impossible to observe the chemical shift anisotropies in most chemical systems. The shielding anisotropies are often large compared to the full range of isotropic shifts for a given nucleus. In randomly oriented solids with more than one structurally distinct species of a given nucleus, individual powder patterns may overlap severely. Extraction of the principal values of the shielding tensors, by pulse techniques alone, may prove to be impossible. To obtain information about chemical shifts in such materials which are in the form of randomly oriented solids, it is necessary to remove both the dipolar broadening and the chemical shift anisotropies. Instead of spinning sufficiently rapidly to average both interactions at the magic angle like E. R. Andrew et al. (23-29) and I. Lowe (30), Schafer et al. (52-54) used a combination of dipolar decoupling and magic angle spinning in cases where the ^{13}C-^{1}H heteronuclear dipolar interaction is the dominant broadening mechanism. The prospects of combining magic angle spinning with homonuclear decoupling were first considered

by Haeberlen and Waugh (35). This experiment was first reported by Gerstein et al. (55), showing the two chemically distinct fluorines in polymerized $FClC{=}CF_2$ to be separated by 23 ppm.

To recover the anisotropic information available in a solid Lippma et al. (56) and Stejskal et al. (57) reported a combined heteronuclear decoupling and sample spinning experiment. By spinning off the magic angle, the powder patterns are scaled by $\frac{(3\cos^2\alpha - 1)}{2}$ such that the individual powder patterns no longer overlap. However, no attempts were made to recover the values of the shielding tensors by fitting the experimental data with an analytical expression for the shielding tensor under rapid sample rotation.

A portion of this thesis deals with the application of combined multiple pulse and sample spinning experiments to samples with protons, which have a larger gyromagnetic ratio (leading to increased homonuclear dipolar broadening) and a smaller range of isotropic chemical shifts as compared to fluorine nuclei. Sample spinning at the magic angle shows the present limits of resolution. In spinning off the magic angle, the first computer fit of an analytical expression to recover the anisotropic shielding information is reported.

These techniques further extend the usefulness of NMR as a microscopic probe sensitive to static and dynamic changes on an atomic scale. The importance of extending these techniques to

the ^{1}H system cannot be underestimated since other techniques usually provide limited information. It is well-known that X-ray diffraction is relatively insensitive in determining hydrogen atom locations. Neutron diffraction experiments usually monitor the ^{2}H isotope because of the large incoherent scattering from ^{1}H. However, in some systems, such as the vanadium hydrogen system, there is a considerable difference between the ^{1}H and ^{2}H phase diagrams (11). In addition, the multiple pulse techniques extend the temperature range over which shielding information may be obtained. With these thoughts, suitable chemical systems were chosen to be studied.

Supported molybdenum catalysts are of current interest because of their importance in hydrodesulfurization and coal hydrogenation (58). Consequently, knowledge about their catalytic properties has become a matter of increasing importance. Toward this end, the reduction of unsupported molybdenum trioxide may provide useful information about the reduction of supported catalysts. As a result, hydrogen molybdenum bronzes (H_xMoO_3) have been the subject of much interest (59-67).

The formation of these bronzes results from the reduction of MoO_3 by hydrogen. For this work, the term bronze may be taken to mean that the basic structure and interatomic bonds of the oxide layers are unaltered by the insertion of hydrogen. While the basic structure remains the same, the overall crystal structure

may be somewhat modified. This definition for bronze is quite similar to that proposed by Suchert (68) in work dealing with interstitial metals.

The MoO_3 crystal (69) consists of distorted MoO_3 octahedra. Each octahedron shares two adjacent edges with its neighbors to form zig-zag chains. These chains are stacked one above the other with each octahedron sharing the apex oxygens with its neighbors in the chains immediately above and below. In this way, layers are formed. These layers are held together by Van der Waal's forces with each layer being offset from its neighbor by a distance equal to half an octahedron. As a result of this structure, there are three types of oxygen atoms when the Mo nearest neighbors are considered. The layered structure consisting of these chains is highly anisotropic.

In the reduced molybdenum trioxide, the nature of the interaction between the inserted hydrogen and the lattice oxygen atoms in the bronzes is not well-understood. Using proton magnetic resonance, Cirillo et al. (59, 60) showed that the bronzes behave as metallic conductors and are comparable to metallic hydrides in electrical conductivity. The NMR spectra were consistent with the interpretation of Sermon and Bond (70) that hydrogen atoms donate an electron to the conduction band of the bronze-forming oxide. In addition, no infrared absorption bands which might be attributable to hydroxyl stretching were

found. However, on the basis of elastic and inelastic neutron studies, Dickens et al. (64) suggested the protons are present as -OH for $H_{0.34}MoO_3$ and as $-OH_2$ for $H_{0.93}MoO_3$, $H_{1.68}MoO_3$ and $H_{2.0}MoO_3$. In addition to the controversy over the nature of the protons, samples of the bronzes used in different studies have been prepared by different methods.

The first method is a "wet" chemistry technique reported by Glemser and Lutz (71). This involves the reduction of MoO_3 by zinc in hydrochloric acid. The "dry" method used by Sermon and Bond (70) uses the hydrogen spillover technique. Powdered MoO_3 in the presence of finely dispersed platinum metal reacts with hydrogen to form the bronze. The hydrogen spillover phenomenon was proposed by Sinfelt and Lucchesi (72) and has been reviewed by various authors (73-76).

Vannice et al. (77) have shown the usefulness of proton NMR in the understanding of the kinetics of the catalytic reduction, via hydrogen spillover, of a similar chemical system, H_xWO_3, by determining the proton mobility. A portion of this thesis deals with the measurement of proton diffusion within the bulk $H_{1.65}MoO_3$, which should aid in the determination of the rate determining step for the formation of $H_{1.65}MoO_3$ by hydrogen spillover. Also, proton NMR with and without strong homonuclear decoupling and sample spinning (at the magic angle as well as at deviations) is used to learn more about the mobility and

nature of protons within the hydrogen molybdenum bronzes. These techniques also allow a comparison of samples of the bronzes prepared by the two different methods.

One of the earliest applications of NMR was the study of a metal hydride, PdH_x, by Norberg (78) in 1952. In the application of NMR to metal hydrogen systems that followed, the NMR measurements, which are sensitive to small changes, were used to locate phase boundaries, determine the hysteresis at phase transitions, and measure the temperature width of a transition. Measurements of relaxation rates and Knight shifts provided information about the electronic structure. In addition, diffusion coefficients were measured to determine mobilities and activation energies. A recent review by Cotts (11) on metal hydrogen systems covers these topics.

In general, proton magnetic resonance provides information on atom locations in a solid through the nuclear dipole interaction. When interactions with paramagnetic ions in the lattice or with the nuclear electric quadrupole are absent, the dipolar field is responsible for the linewidth (and second moment) of the resonance. By agreement between the experimental second moment and the calculated second moment based on a suitable model, the location of the protons may be inferred. Even with the absence of the large interactions due to paramagnetic ions or nuclei with large quadrupole moments, contributions to the linewidth and

second moment result from atomic motion. Measurements of the spin-lattice relaxation time, the spin-spin relaxation time, and the rotating frame spin-lattice relaxation time indicate the size of these contributions. In addition, if the protons do not reside in sites of cubic symmetry, a contribution to the linewidth from Knight shift anisotropy may result. Lau et al. (47) used a variety of NMR techniques, including multiple pulse homonuclear decoupling, to look at the specific contributions of various interactions.

Anderson et al. (79-81) have used conventional wideline NMR to determine the proton locations in the β-phase (dihydride) of YH_x (82) from the second moment. In β-YH_x, the hydrogen resides in the interstitial tetrahedral and octahedral sites of the fcc Y-lattice. The rigid lattice second moment is sensitive to the distribution of hydrogen atoms in these sites. β-YH_x presents a favorable case for this method since the contribution to the second moment from the metal nuclei (^{89}Y) is negligible due to the very small nuclear dipole moment of ^{89}Y (roughly 5% that of the proton). Also, if the protons reside at the centers of the sites, the cubic symmetry excludes the possibility of Knight shift anisotropy. The occupancy factors determined from the broadline NMR studies are in reasonable agreement with those obtained by neutron diffraction (83). Since there are experimental errors in both measurements, a portion of this thesis deals with

the application of multiple pulse techniques to provide more information on the environment of protons in $YH_{1.92}$ by quantifying the contribution to the second moment from interactions other than the homonuclear dipolar interaction.

Electron spin resonance using dilute Er ions in β-YH_x has been used to infer site energies (84) of the proton distribution. Anderson et al. (81) have found three distinct regions for which the activation energy for hydrogen diffusion increases with temperature. These results lead to speculation that motion may occur only on one sublattice, then exchange between tetrahedral and octahedral site hydrogens, and finally motion of all hydrogen on both sublattices. This work also found the quantity $(T_{1e}T)^{-\frac{1}{2}}$, which is proportional to the density of states at the Fermi level, to be a constant for the range of compositions in the dihydride phase. It also suggested that a previous study (85) is in error because of the presence of a substantial level of paramagnetic impurities. This thesis also reports the measurement of the Knight shift using the combined multiple pulse and magic angle spinning experiment to further aid in the understanding of the electronic structure.

BASIC THEORY

A wide variety of NMR measurements ranging from simple relaxation studies to multiple pulse spectra have been used to study protons in $H_{1.7}MoO_3$ and $YH_{1.92}$. For this reason, this section presents an overview of the basic theories used in the interpretation of these data.

A nucleus of spin I has 2I + 1 energy levels. When placed in a static magnetic field H, these levels are separated by

$$\Delta E = \mu H/I \tag{1}$$

where the nuclear magnetic moment is given by

$$\mu = \gamma \hbar I \tag{2}$$

Here γ is the gyromagnetic ratio and $\hbar$ is Planck's constant divided by 2π. A transition between adjacent levels occurs when the frequency of the applied radiation is

$$\omega = \gamma H \text{ (rad/sec)} \tag{3}$$

At equilibrium, the nuclei are distributed among the energy levels according to a Boltzmann distribution. When the macroscopic magnetization in the presence of the static magnetic field is disturbed from equilibrium by a radiofrequency pulse, Bloch et al. (15) found that the motion of this magnetization is given by the phenomenological differential equation

$$\frac{d\vec{M}}{dt} = \gamma \vec{M} \times \vec{H}, \tag{4}$$

where $\vec{M}$ is the vector sum of the μ's, as the magnetization relaxes to equilibrium.

Bloembergen et al. (17) put relaxation effects on a more theoretical basis by considering the exchange of energy between a system of nuclear spins in a static magnetic field with the heat reservoir consisting of the other degrees of freedom (lattice) of the material. By considering the dipolar Hamiltonian for the nuclear spin system, the spin-lattice relaxation rate for identical nuclei can be written as

$$\frac{1}{T_1} = \frac{3}{2}\gamma^4\hbar^2 I(I+1)\{J_1(\omega) + J_2(2\omega)\} \tag{5}$$

The spectral densities are given by

$$J_i(\omega) = \int_{-\infty}^{\infty} K_i(\tau)\exp(i\omega\tau)d\tau \tag{6}$$

where the correlation functions $K_i(\tau)$, related to the phase memory time for the molecular motions, are defined as

$$K_i(\tau) \equiv \overline{Y_i(t)Y_i^*(t+\tau)} \tag{7}$$

The Y_i^* is the complex conjugate of Y_i, defined by

$$\begin{aligned} Y_0 &= r^{-3}(1 - 3\cos^2\theta) \\ Y_1 &= r^{-3}\sin\theta\cos\theta\exp(i\phi) \\ Y_2 &= r^{-3}\sin^2\theta\exp(2i\phi) \end{aligned} \tag{8}$$

The bar over the Y's indicates an average over the ensemble of nuclei. This theory provides the basis for most modern spin-lattice relaxation theories and, in particular, was used for the analysis of T_1 data in this thesis.

However, other interactions may also provide mechanisms for spin-lattice relaxation. Specifically, a conduction electron component $(\frac{1}{T_1})_e$ to the spin-lattice relaxation rate in

metallic conductors is produced by the electronic structure through the time dependence of the transverse components of the hyperfine fields produced at the site of the nucleus. The rate $(\frac{1}{T_{1e}})$ is proportional to the absolute temperature. At very low temperatures, where the nuclear dipolar interaction fails to provide an effective relaxation mechanism, the spin-lattice rate is essentially entirely due to the coupling of the nuclei to the magnetic moment of the S-state electrons. The Korringa relation (86), which applies only to S contact hyperfine interaction and effectively free electron metals, is given by

$$K^2(T_{1e}T) = \text{constant}, \tag{9}$$

where K is the Knight shift.

One of the most important discoveries was that of the spin echo by Hahn (87). Following a $\frac{\pi}{2}$ pulse, the transverse magnetization dephases under a static field inhomogeneity. Applying a π pulse at a time τ after the $\frac{\pi}{2}$ pulse causes the magnetization to refocus at a time 2τ in the absence of interactions not proportional to I_z. Hahn showed the translational motion contributes to the decay of the amplitude of the echo in addition to the normal spin-spin interactions. The amplitude for a $\frac{\pi}{2}$-τ-π sequence is given by

$$M(2\tau) = M(0)\exp\{-\frac{2\tau}{T_2} - \frac{2}{3}\gamma^2G^2D\tau^3\}, \tag{10}$$

where G is the spatial magnetic field gradient and D is the diffusion coefficient. In samples with long spin-spin relaxation

times (on the order of milliseconds), the τ^3 dependence is pronounced for large values of τ. Carr and Purcell (49) showed that a sequence of π pulses following the $\frac{\pi}{2}$ pulse reduces the effects of diffusion with the amplitude of the echo occurring at a time $t = 2n\tau$ given by

$$M(t) = M(o)\exp\{-\frac{t}{T_2} - (\tfrac{1}{3})\gamma^2G^2D\tau^2t\}. \qquad (11)$$

The rate constant of the diffusion term, $\frac{1}{T_2'} = \frac{1}{3}D\gamma^2G^2\tau^2$, can be made arbitrarily small by making the 2τ intervals between the π pulses arbitrarily small. Comparing the results of both experiments and solving equations (10) and (11) simultaneously gives the product of G^2D. Knowledge of the diffusion coefficient allows the determination of the background gradient within the sample.

Stejskal and Tanner (88) deliberately introduced a pulsed field gradient into the spin echo experiment in order to measure D. A constant gradient G is applied for a time δ between the $\frac{\pi}{2}$ and π pulses and between the π pulse and the formation of the echo. The constant background gradient G_o includes the magnet inhomogeneity and the internal demagnetization fields. The attenuation of the echo for the pulsed gradient is given by

$$M(2\tau) = M_o' \exp[-\gamma^2D\{(\tfrac{2}{3})\tau^3G_o^2 + \delta^2(3\Delta - \delta)\frac{G^2}{3}$$
$$-\delta[(t_1^2 + t_2^3) + \delta(t_1 + t_2) + \frac{(2\delta^2)}{3} - 2\tau^2]\vec{G}\cdot\vec{G}_o\}] \qquad (12)$$

where Δ is the time between gradient pulses, $t_2 = 2\tau - (t_1 + \Delta + \delta)$,

and M_o' includes the T_2 term. In many experiments the G^2 term can be made much larger than $(\vec{G}\cdot\vec{G}_o)$. The $(\vec{G}\cdot\vec{G}_o)$ term may be neglected provided $\frac{|\vec{G}|}{|\vec{G}_o|} >> \frac{\tau}{\delta}$. When this condition is met and $M_o'' \equiv M_o' \exp[-\gamma^2 D\tau^3 G_o^2(\frac{2}{3})]$, a constant, then the echo attenuation is

$$\frac{M(2\tau)}{M_o''} = \exp[-\gamma^2 D\delta^2 G(\Delta - \tfrac{1}{3}\delta)]. \qquad (13)$$

Determination of the strength of the applied gradient G from a standard allows the measurement of D.

The multiple pulse experiments are best explained through the application of average Hamiltonian theory (35, 36, 39) to the behavior of the nuclear spin system under a radiofrequency pulse sequence. The time evolution of the nuclear spin system is governed by the time evaluation of the density matrix operator, ρ, which obeys (89) the equation

$$i\frac{d\rho}{dt} = [H, \rho], \qquad (14)$$

in units such that $\hbar = 1$, with H being the spin Hamiltonian. In the interaction frame of the Zeeman Hamiltonian, the spin Hamiltonian is given by

$$H(t) = H_{int} + H_{rf}(t). \qquad (15)$$

In the absence of nuclear quadrupole interactions, of motion, and of heteronuclear dipolar interactions, the internal Hamiltonian has no explicit time dependence and is given by

$$H_{int} = (\omega - \omega_o)I_z - \omega_o\Sigma\sigma_{zzi}I_{zi} + \Sigma\Sigma_{i<j} B_{ij}(r_{ij})(\vec{I}_i\cdot\vec{I}_j - 3I_{zi}I_{zj}) \qquad (16)$$

where ω_o is the resonant frequency, σ_{zzi} describes the electronic shielding of the i^{th} nucleus, and $B_{ij}(r_{ij})$ contains the spatial portion of the homonuclear dipolar interaction. $H_{rf}(t)$ is strongly time dependent and provides the major perturbation to the nuclear spin system.

The solution of equation (14) is given by

$$\rho(t) = U(t,o)\rho(o)U^{+}(t,o) \tag{17}$$

where the time development operator can be written as

$$U(t,o) = U_{rf}(t,o)U_{int}(t,o)$$

and the $U_i(t, o)$ are determined by the solution of

$$i\frac{dU_i(t)}{dt} = H_i U_i(t). \tag{18}$$

The solutions to equation (18), given by the Dyson expression (89), are

$$U_{rf}(t,o) = T\exp[-i\int_o^t H_{rf}(t')dt'] \tag{19}$$

and

$$U_{int}(t,o) = T\exp[-i\int_o^t \tilde{H}_{int}(t')dt'] \tag{20}$$

where T is the Dyson time ordering operator and

$$\tilde{H}_{int}(t) = U_{rf}^{+}(t,o)H_{int}U_{rf}(t,o). \tag{21}$$

If the $H_{rf}(t)$ is periodic

$$H_{rf}(t + Nt_c) = H_{rf}(t), \tag{22}$$

where Nt_c represents integral multiples of the cycle time, and cyclic

$$\int_o^{Nt_c} H_{rf}(t)dt = 0, \tag{23}$$

the $\tilde{H}_{int}$ becomes periodic as well. From equations (19) and (23),

$$U_{rf}(Nt_c,0) = T\exp(0) = 1, \tag{24}$$

and then

$$U_{int}(Nt_c, 0) = [U_{int}(t_c, 0)]^N. \tag{25}$$

Using the Magnus expansion (90),

$$U_{int}(Nt_c, 0) = \exp[-iNt_c(\bar{H}^{(0)}_{int} + \bar{H}^{(1)}_{int} + \bar{H}^{(2)}_{int} + \ldots)], \tag{26}$$

where

$$\bar{H}^{(0)}_{int} = \frac{1}{t_c}\int_0^{t_c} \tilde{H}_{int}(t')dt' \tag{27}$$

$$\bar{H}^{(1)}_{int} = \frac{-i}{2t_c}\int_0^{t_c} dt'' \int_0^{t''} dt' [\tilde{H}_{int}(t''), \tilde{H}_{int}(t')] \tag{28}$$

$$\bar{H}^{(2)}_{int} = \frac{1}{t_c}\int_0^{t_c} dt''' \int_0^{t'''} dt'' \int_0^{t''} dt' \{[\tilde{H}_{int}(t'''), [\tilde{H}_{int}(t''),$$

$$\tilde{H}_{int}(t')]] + [\tilde{H}_{int}(t'), [\tilde{H}_{int}(t''), \tilde{H}_{int}(t''')]]\}. \tag{29}$$

The strong condition for convergence of this series is

$$t_c \| \tilde{H}_{int}(t) \| \ll 1. \tag{30}$$

At times $t = Nt_c$, the density matrix behaves as if it develops under an "average" Hamiltonian

$$\bar{H}_{int} = \bar{H}^{(0)}_{int} + \bar{H}^{(1)}_{int} + \bar{H}^{(2)}_{int} + \ldots. \tag{31}$$

which is time independent. Hence, the set of interaction Hamiltonians given by equation (16) is not unalterable. Specific pulse sequences can be used to suppress the effects of a particular Hamiltonian to obtain the information contained in another. The results of the application of average Hamiltonian theory to the MREV 8 pulse (40, 41, 44), the Burum and Rhim 24 pulse (43), and the dipolar narrowed Carr-Purcell (49) sequences have been given in the literature.

Multiple pulse NMR allows the measurement of the chemical shift interaction in many chemical systems where this information has been obscured by dipolar broadening. The electronic shielding of nuclei is one of the most important pieces of information to chemists, since it elucidates the local environment of the nucleus, i.e., indicates molecular structure. The shielding Hamiltonian, expressed in irreducible spherical tensors, has the form (12)

$$H_\sigma = \gamma \sum_{\ell=0,2} \sum_{m=-\ell}^{\ell} (-1)^m T_{\ell,m} \sigma_{\ell,-m} \tag{32}$$

where the $T_{\ell,m}$ describe the spin variables and the $\sigma_{\ell,-m}$ describe the components of the second rank shielding tensor. The nonzero components in the tensor's principal axis system (PAS), denoted by $\rho_{\ell,m}$, are related to the PAS $\sigma_{\alpha\alpha}$ by

$$\begin{aligned} \rho_{0,0} &= \tfrac{1}{3}\mathrm{Tr}\underline{\underline{\sigma}} \\ \rho_{2,0} &= \tfrac{\sqrt{3}}{2}(\sigma_{33} - \tfrac{1}{3}\mathrm{Tr}\underline{\underline{\sigma}}) = \tfrac{\sqrt{3}}{2}\delta \\ \rho_{2,\pm 2} &= \tfrac{1}{2}(\sigma_{22} - \sigma_{11}) = \tfrac{1}{2}\eta\delta. \end{aligned} \tag{33}$$

The $\rho_{\ell,m}$ can be expressed in the LAB system by

$$\sigma_{\ell,-m}^{(\mathrm{LAB})} = \sum_{m'} D_{m,-m}^{\ell}(\alpha,\beta,\gamma)\rho_{\ell,m'} \tag{34}$$

where α,β,γ represent the Euler angles by which the LAB system is brought into coincidence with the PAS. Substitution of equations (33) and (34) into equation (32) gives

$$H_\sigma = \omega_o I_z\{\tfrac{1}{3}Tr\underline{\underline{\sigma}} + \tfrac{\delta}{2}((3\cos^2\beta - 1) + \eta\sin^2\beta\cos 2\gamma)\}. \qquad (35)$$

When the sample is rotated with frequency ω_r about an axis inclined at an angle θ away from the static magnetic field, two transformations are needed to relate $\underline{\underline{\sigma}}$(PAS) to the $\underline{\underline{\sigma}}$(LAB). The equation (34) becomes

$$\sigma_{\ell,-m}(LAB) = \sum_{m'} D^{\ell}_{m',-m}(0,\theta,\omega_r t)\sum_{m''} D^{\ell}_{m'',m'}(\Omega')\rho_{\ell,m''} \qquad (36)$$

where Ω' represents the Euler angles which bring the PAS into coincidence with the sample spinning coordinate system. After time averaging, the shielding Hamiltonian is given by

$$H_\sigma = \omega_o I_z\{\tfrac{1}{3}Tr\underline{\underline{\sigma}} + \tfrac{1}{2}(3\cos^2\theta - 1)\cdot\tfrac{\delta}{2}[(3\cos^2\beta - 1) + \eta\sin^2\beta\cos^2\gamma]\}. \qquad (37)$$

Pembleton (91) has shown that "time averaging" is equivalent to spinning at $\omega_r >> (\sigma_{zz} - \frac{1}{3}Tr\underline{\underline{\sigma}})$ by calculating the expectation value of the nuclear spin operator I_y. In addition, Pembleton (91) has discussed the interaction between the homonuclear decoupling and magic angle spinning. If the rotational cycle time t_r is long compared to the multiple pulse cycle time t_c, there is no interaction between the two experiments with respect to the dipolar decoupling. In general, dipolar broadening on the order of 20,000 Hz and stable rotation speeds of less that 4,000 Hz are sufficient for meeting this condition.

EXPERIMENTAL

NMR Spectrometer

With the development of Fourier transform NMR, the pulse sequences used for NMR experiments have progressed from simple sequences to measure relaxation times to the complicated multiple pulse sequences for homonuclear decoupling. As the chemical systems became more difficult to study [in terms of shorter multiple pulse cycle times needed for protons in rigid solids with short spin-spin relaxation times, or in terms of signal-to-noise ratio needed for observing residual protons in such systems as SiO_2-Al_2O_3], the technical challenges resulting from the desire to study these systems place more stringent requirements on the spectrometer.

The pulsed NMR spectrometer is a broad band, high power (~500 watts) unit similar to those discussed by Ellet et al. (92) and by Rhim et al. (41). Operating at a frequency of 56 MHz for protons with a deuterium lock for magnetic field stabilization, the spectrometer takes advantage of tuned circuits wherever possible to improve signal-to-noise, as shown in Figure 1. However, the Q's have been purposefully kept low, while sacrificing signal-to-noise, to minimize transients.

The receiver consists of three stages, the first being an Avantek Model 511 amplifier with the next two being Spectrum

Figure 1. Block diagram of multiple pulse spectrometer used for homonuclear decoupling experiments

MULTIPLE PULSE SPECTROMETER

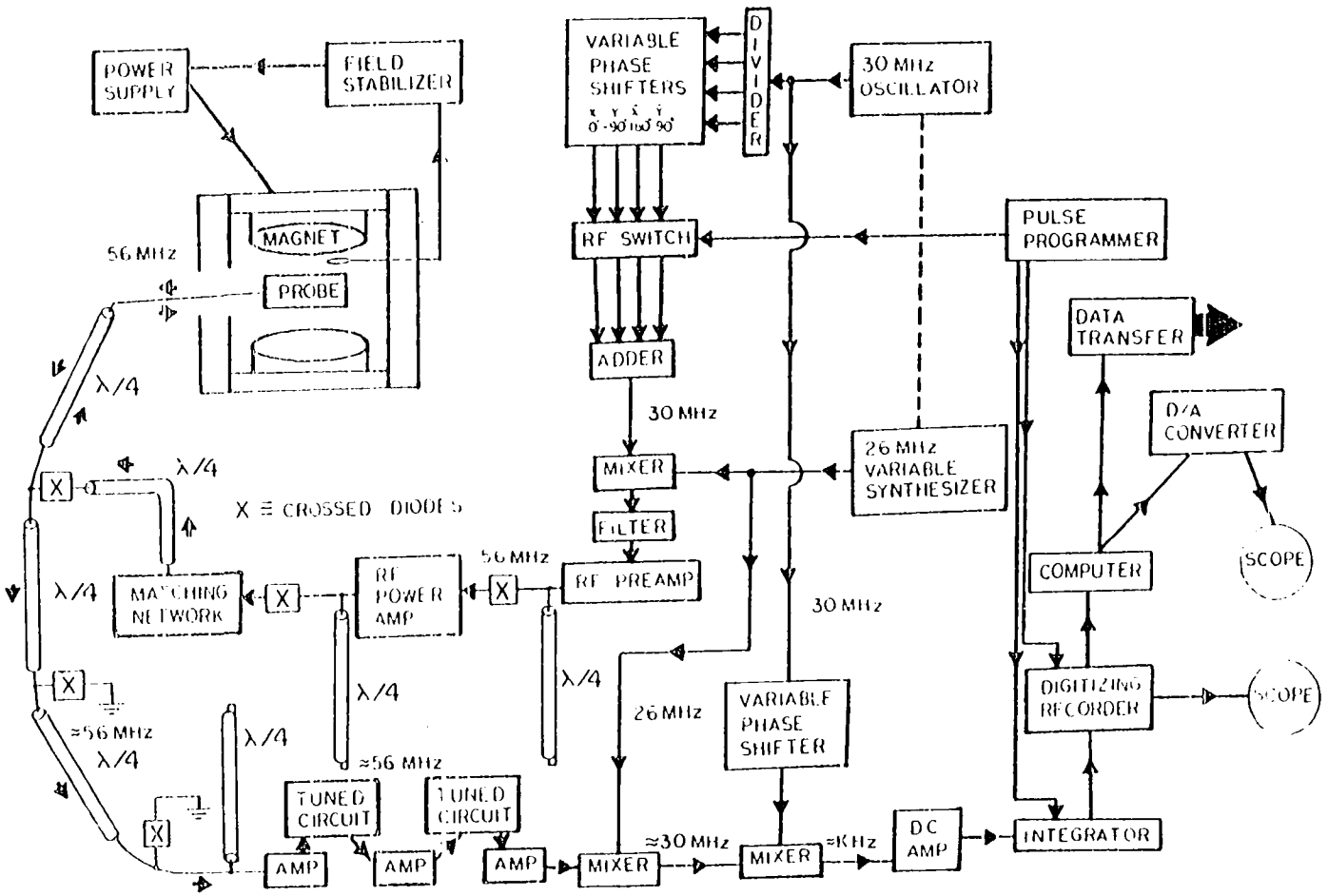

Microwave Model SMLD-10 limiting amplifiers, with a total gain of approximately 60 db. Following a 1.5 usec pulse, the dead time of the receiver before recovery of a NMR signal is approximately 3.5 usec. This period is dominated by probe ringdown. The transient recorder is a Biomation 805, with a minimum sampling time of 0.2 usec per channel. The memory of the unit contains 2048 eight-bit words. The Biomation is interfaced to a PDP 11/10 computer for signal averaging and data manipulation.

The transmitter is an IFI model 404 distributed amplifier system capable of 500 watts in pulsed operation. With proper matching of the transmitter to the probe by a π circuit to symmetrize and minimize phase transients and with a probe of Q less than 30, $\frac{\pi}{2}$ pulse widths of $\sim$1.0 usec can be attained. Care was taken to maximize the homogeniety of the H_1 field produced by the probe.

The pulse programmer allows the utilization of multiple pulse sequences requiring four different radiofrequency phases. The unit has four channels with analogue control of pulse widths, three channels with digital control of pulse widths and 0.1 usec resolution, and three channels used as triggers for experimental events. It is based on a Motorola 6800 microprocessor system and has been previously described (93).

The NMR probes made use of standard tapped-series tuned circuits. A gas flow system was used to vary temperatures.

The sample spinning probe (94) and sealable rotors (95) for oxygen and water sensitive compounds have been described elsewhere.

The ability of the NMR spectrometer to remove homonuclear dipolar interactions has been determined (96) by utilizing the MREV-8 cycle (40, 44) on ^{19}F with the external field along the [111] direction of a cylindrical single crystal of CaF_2. A linewidth of 34 Hz was obtained in such measurements.

Pulse Gradient Unit and Probe

The resonant circuit for the NMR measurement in the probe used for diffusion measurements is also a standard tapped series tuned circuit. The magnetic field gradient is supplied by a quadrupole coil constructed according to the design of D. S. Webster and Marshen (97). The gradient coil is 4 cm long, has an average i.d. of 15 mm, and is wound with 10 turns per quadrant. The total inductance is 4μH. The coil constant, calibrated by the method of Stejskal and Tanner (88) using water and glycerol as standards [taken to be 3.2×10^{-8} cm^2/sec for glycerol (98, 99) and 2.35×10^{-5} cm^2/sec for water (100, 101)] is 9.35 (G/cmA). The pulse gradient unit is similar in design to that given in reference 101. Gradients of 100 G are achieved in gradient pulses of 20 usec in duration. Temperature is controlled by air flow through a annular

"race track" groove machined in a cylindrical aluminum block in which are inserted the quadrupole and NMR coils.

Preparation of $H_{1.7}MoO_3$

The hydrogen molybdenum bronze $H_{1.7}MoO_3$ may be prepared by the "wet chemistry" method of Glemser and Lutz (71). In this preparation, 10.0 g of MoO_3 (ACS, 99.5%) and 3.0 g of granulated Zn were pumped in vacuum in a 200 ml round bottom flask with a stopcock side-arm. Dry nitrogen gas was bubbled through concentrated HCl and through H_2O to displace oxygen. Under a nitrogen atmosphere, 50 ml H_2O and 10 ml HCl were added. The mixture was stirred overnight.

Using a filter stick, the mixture was filtered under a nitrogen atmosphere. The product was washed four times with distilled, degassed H_2O. The mother liquor was tested for Cl^- by adding $AgNO_3$. When no white precipitate formed, the blue product was dried under vacuum over P_2O_5.

In the hydrogen spillover method (70), the platinum was dispersed within the powdered molybdenum trioxide by impregnation with the appropriate volume of a 0.21 M solution of H_2PtCl_6 prepared using distilled, deionized water. The solution was diluted to about 30 ml and 20.0 g of MoO_3 powder was added while stirring. The slurry was hand stirred and heated gently over a hot plate until the solution evaporated. Any clumps were broken as they formed. The material was then

heated to 120°C in air overnight. The sample prepared in this manner contained 2.0% Pt by weight. The hydrogen molybdenum bronze was prepared by exposing the above mentioned Pt/MoO_3, previously evacuated at 60°C for one hour, to dry hydrogen gas. A liquid nitrogen trap was kept between the gas handling system and the reactor. The bronze has been reported to be formed in less than thirty minutes (14). The sample was allowed to sit in hydrogen for three hours to assure equilibrium.

The stoichiometries of the samples were verified by proton spin counting (102). The "wet" sample was determined to be $H_{1.74(\pm 0.15)}MoO_3$. The sample prepared using the dry hydrogen spillover technique was found to have the stoichiometry $H_{1.66(\pm 0.15)}MoO_3$.

RESULTS AND DISCUSSIONS

Combined Multiple Pulse NMR and Sample Spinning

The usefulness of the combined multiple pulse NMR and sample spinning experiment to provide chemical information is easily demonstrated. The ^1H NMR absorption spectrum of 2,6-dimethylbenzoic acid from a homonuclear decoupling experiment is shown in Figure 2. The lack of distinct spectral features results from the overlap of the chemical shift tensors of the acid, aromatic, and aliphatic protons.

In contrast, the ^1H NMR absorption spectrum for the same compound obtained using the Burum and Rhim 24 pulse sequence (43) and a magic angle rotation speed of approximately 3 kHz has been previously reported (103) and is shown in Figure 3. The shifts corresponding, in order of decreasing shielding, to the aliphatic, aromatic, and carboxylic acid protons are clearly distinguishable. The experimental areas of 5.6:2.7:1.7 are in fair agreement with the 6:3:1 ratio expected for the aliphatic, aromatic, and acid protons. The solid state spectrum shows a difference from that obtained in solution. In dilute deuterated acetone, the carboxylic acid proton chemical shift is at -10.7 ppm relative to TMS. In the solid, this resonance occurs at -14.8 ppm. This downfield displacement of the resonance signal simply reflects the well-known formation of hydrogen-bonded dimers in the solid form of carboxylic acids (104).

Figure 2. ^{1}H NMR absorption spectrum of 2,6-dimethylbenzoic acid under a homonuclear decoupling experiment without sample spinning

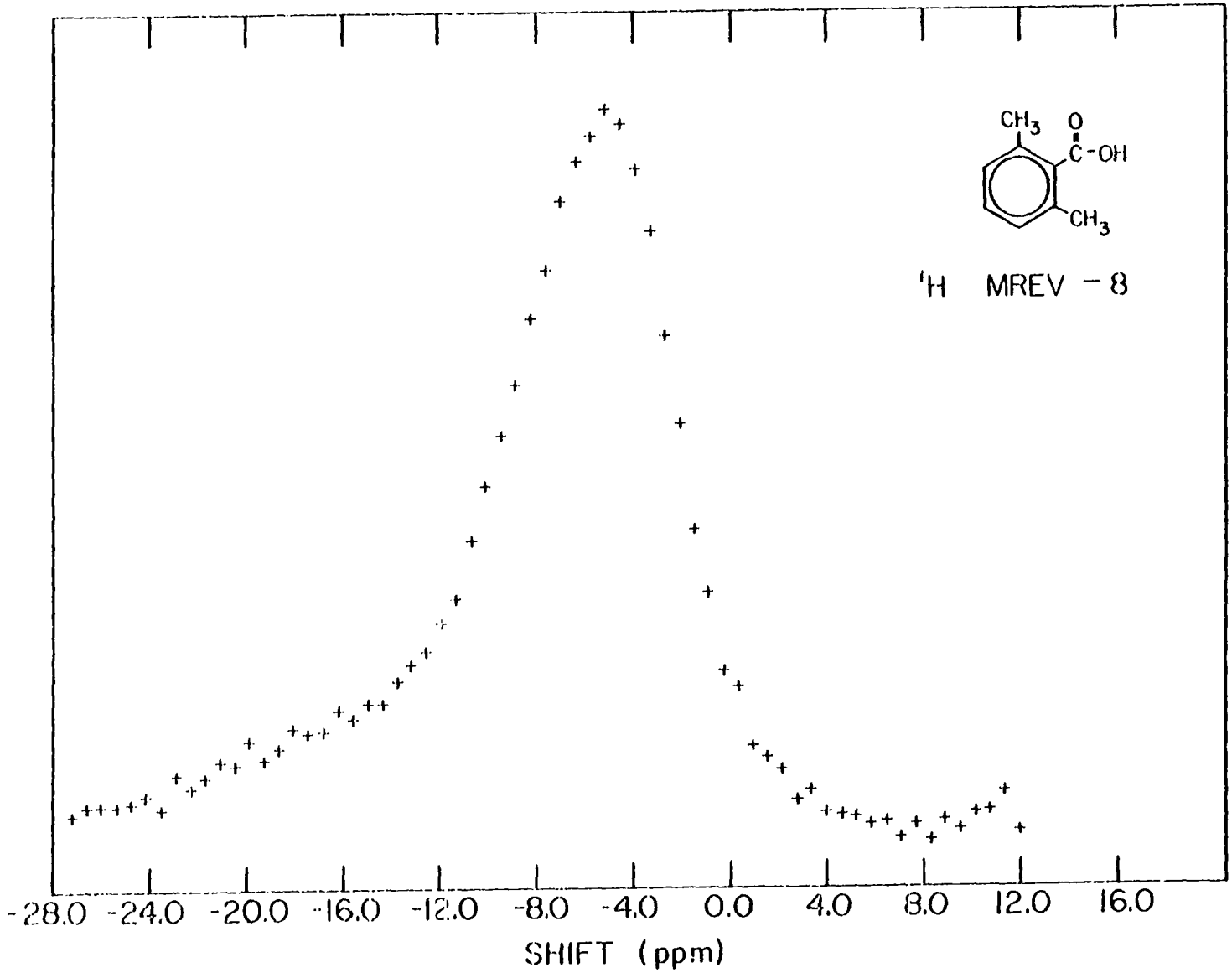
CH3
O
C-OH
CH3
^{1}H MREV – 8
-28.0 -24.0 -20.0 -16.0 -12.0 -8.0 -4.0 0.0 4.0 8.0 12.0 16.0
SHIFT (ppm)

Figure 3. Combined multiple pulse ^{1}H NMR and magic angle spinning spectrum of 2,6-dimethylbenzoic acid (Referenced to H_2O. $\sigma_{TMS}-\sigma_{H_2O}$ = 4.58 ppm)

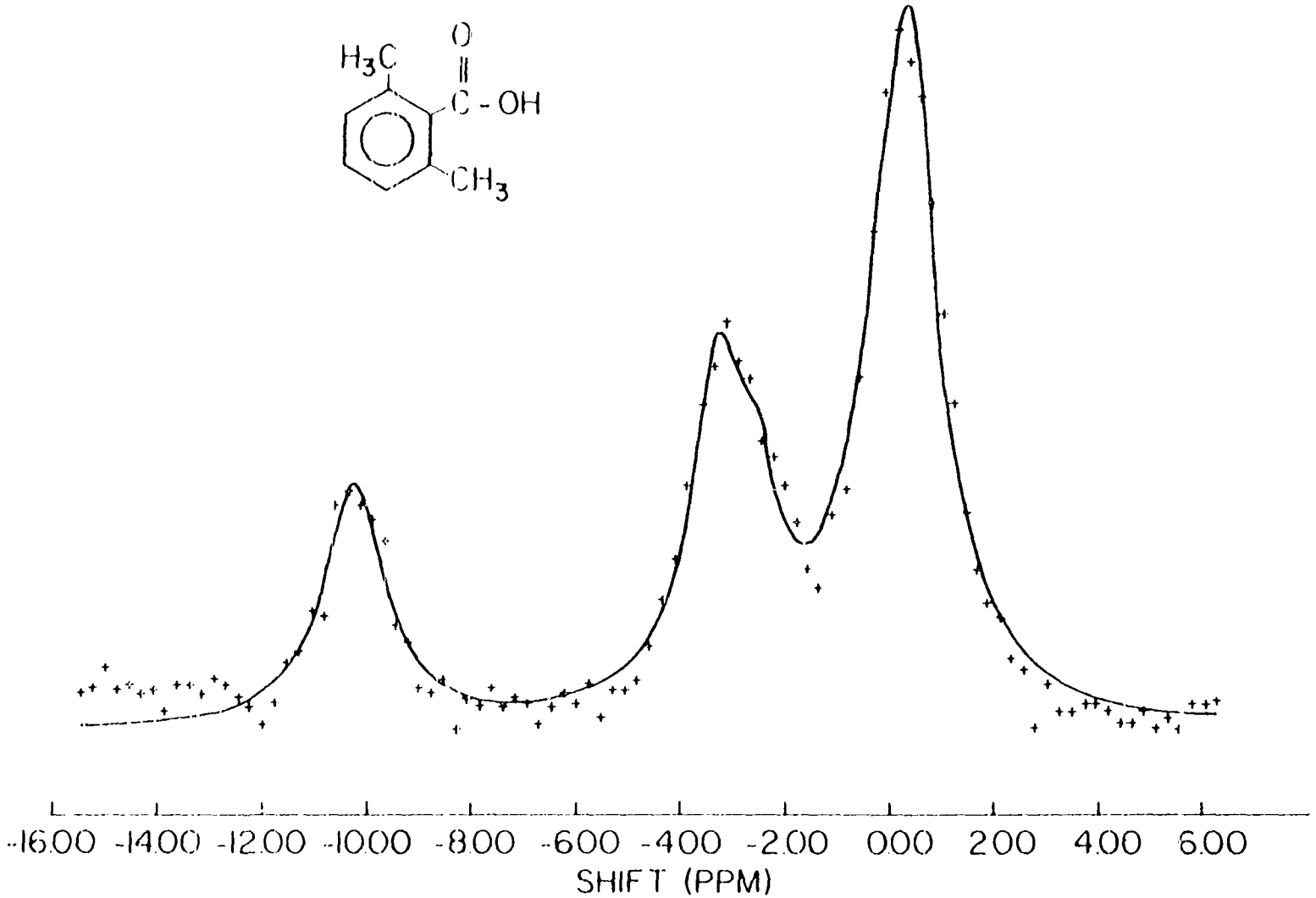
H3C
O
C - OH
CH3
-16.00 -14.00 -12.00 -10.00 -8.00 -6.00 -4.00 -2.00 0.00 2.00 4.00 6.00
SHIFT (PPM)

The ^1H NMR absorption spectrum of 2,6-dimethylbenzoic acid under combined homonuclear decoupling and sample spinning at $\theta = 75°$ has been previously reported (105) and is shown in Figure 4(a). The peaks at about -13, -8, and -4 ppm with respect to TMS may be identified with the acid, aromatic, and aliphatic protons respectively. A lineshape associated with axially symmetric chemical shift anisotropy is clearly evident for the acid protons.

The chemical shift tensor orientation is described by the solid angle Ω. In powdered samples, all angles Ω are equally probable and the lineshape is generated by summing over all possible orientations. If the chemical shift powder pattern is assumed to be broadened by a Lorentzian broadening function, one obtains

$$I(\omega) = \int_0^{2\pi}\int_0^{\pi}\{\frac{[\omega(\beta,\gamma) - \omega]^2}{W^2} + 1\}^{-1}\sin\beta d\beta d\gamma \qquad (38)$$

where $\omega(\beta,\gamma)$, recalling equation 37, is given by

$$\omega(\beta,\gamma) = \omega_o\{\tfrac{1}{3}\mathrm{Tr}\underline{\underline{\sigma}} + \tfrac{1}{2}(3\cos^2\theta - 1)\cdot\tfrac{\delta}{2}[(3\cos^2\beta - 1) + \eta\sin^2\beta\cos 2\gamma]\} \qquad (39)$$

with θ as the angle between the axis of rotation and the static magnetic field. Under rapid sample rotation, the spectrum is scaled by a factor of $\frac{1}{2}(3\cos^2\theta - 1)$.

An expanded version of the spectrum of 2,6-dimethylbenzoic acid illustrating the computer fit of equation 38 for the axially symmetric case ($\eta = 0$) to the experimental data for the acid

Figure 4a. ^1H NMR absorption spectrum of 2,6-dimethylbenzoic acid under combined homonuclear decoupling and sample spinning at $\theta = 75°$

Figure 4b. Enlarged portion of the same spectrum corresponding to the carboxyl ^1H chemical shift tensor

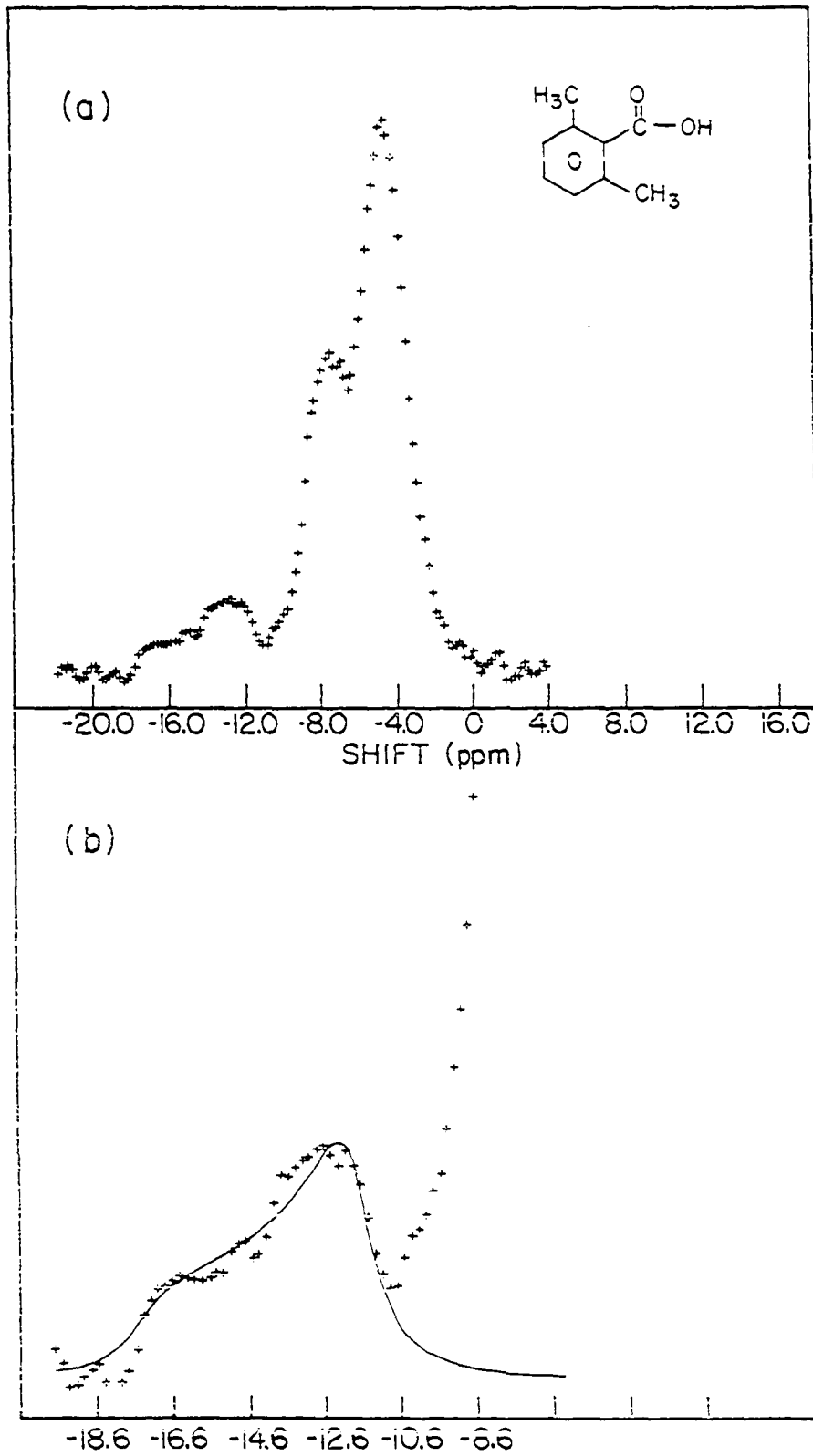
(a)
H3C
O
C—OH
CH3
-20.0 -16.0 -12.0 -8.0 -4.0 0 4.0 8.0 12.0 16.0
SHIFT (ppm)
(b)
-18.6 -16.6 -14.6 -12.6 -10.6 -8.6

protons is shown in Figure 4(b). For $\theta = 75°$, the scaling factor $\frac{1}{2}(3\cos^2\theta - 1)$ is approximately -0.4. The experimental anisotropy $\Delta\sigma = \sigma_{\parallel} - \sigma_{\perp} = -5.7$ ppm is indeed scaled by about this amount (including sign reversal) when compared with previously reported carboxylic acid ^1H tensors. The principal values, obtained via the computer fit of equation 38 to the experimental data, are $\sigma_{\perp} = -18.5$ ppm and $\sigma_{\parallel} = -4.2$ ppm, relative to TMS, yielding an anisotropy of +14.3 ppm.

The anisotropy reported above for carboxylic acid protons in 2,6-dimethylbenzoic acid is 2.5 ppm less than the smallest previously reported anisotropy for protons in a carboxylic acid (106). In order to check the viability of the combined multiple pulse and sample spinning technique for quantitative determinations of proton chemical shift tensors, the ^1H chemical shift anisotropy was also measured for squaric acid using the Burum and Rhim 24 pulse cycle with, and without, sample spinning. Squaric acid contains only one type of proton, the carboxylic acid proton, and has been investigated several times in the past, both as a powder (107) and in single crystals (108). Table I compares the values obtained with those previously reported. Within experimental error (±1 ppm on any tensor component), the values inferred from the spinning and static experiments are in good agreement, and the anisotropy compares favorably with that previously measured in powdered squaric acid. However, it is

Table I. Carboxyl ^1H chemical shift tensors[a]

Sample	σ_{11}	σ_{22}	σ_{33}	σ_{iso}[b]	$\Delta\sigma$[c]	Method[d]	Reference
Squaric acid	-22.5	-22.5	-0.1	14.6	22.4	MP,PW	This work
	-21.7	-21.7	-0.2	-14.5	21.5	MP,SS,PW	This work
	-18.5	-18.5	3.5	-11.2	22.0	MP,PW	107
	-26.5	-20.2	1.0	-15.2	27.5	MP,SC	108
2,6-DMBA[e]	-18.5	-18.5	-4.2	-13.7	14.3	MP,SS,PW	This work

[a]Reference is in ppm relative to TMS.

[b]$\sigma_{iso} = \frac{1}{3}(\sigma_{11} + \sigma_{22} + \sigma_{33})$.

[c]$\Delta\sigma = (\sigma_{33} - \sigma_{11})$

[d]MP, multiple pulse; PW, powder spectra; SS, sample spinning; SC, single crystal.

[e]2,6-dimethylbenzoic acid.

seen that only the single crystal study was able to clearly distinguish the nonaxial symmetry of the tensor. Within the accuracy obtainable with powder samples, then, the spinning results appear to be as reliable as in the case of static samples. In view of the experimental error, the isotropic value of -13.7 ppm obtained from fitting the scaled tensor is in reasonably good agreement with -14.8 ppm obtained from the magic angle spinning experiment.

Nature and Mobility of Protons in $H_{1.7}MoO_3$

The X-ray photoelectron (XPS) spectra of the core 3d electrons of Mo in the two samples prepared by the wet and the

dry methods are shown in Figure 5(a) and 5(b) respectively. These data were obtained using an AEI ES200B spectrometer with Al K_α monochromatic radiation (1486.6 eV) with a maximum resolution of 0.5 eV. The solid lines were generated by APES (109), a computer program to Analyze Photo Electron Spectra.

Sermon and Bond (70) point out that the average oxidation state of molybdenum should decrease from +6 in MoO_3 to +5 in $HMoO_3$ and to +4.3 in $H_{1.7}MoO_3$. The average values could arise from the summation of suitable fractions of Mo^{+6}, Mo^{+5}, Mo^{+4}, or other oxidation states. If the $H_{1.7}MoO_3$ contains a mixture of empty, singly, and doubly filled interstices, one would expect the major ionic species to be Mo^{+4}, plus a smaller amount of Mo^{+6} and Mo^{+5}. This model of three different oxidation states for Mo, allowing amplitudes, positions, and full widths at half maximum (FWHM) to vary, was used to interpret the observed XPS data. The results are given in Table II. The results of K. S. Kim et al. (110) and Cimino and DeAngelis (111) are given in Table III.

The $3d_{\frac{5}{2}}$ - $3d_{\frac{3}{2}}$ peaks for Mo^{+4} are found at the appropriate binding energies. The fitted areas indicate that the majority of the Mo detected is present as Mo^{+4}. The FWHM is in reasonable agreement with that reported by Kim et al. for MoO_2. However, the rather broad FWHM for types II and III are consistent with a range of oxidation states for the "Mo^{+5}" and "Mo^{+6}" assignments.

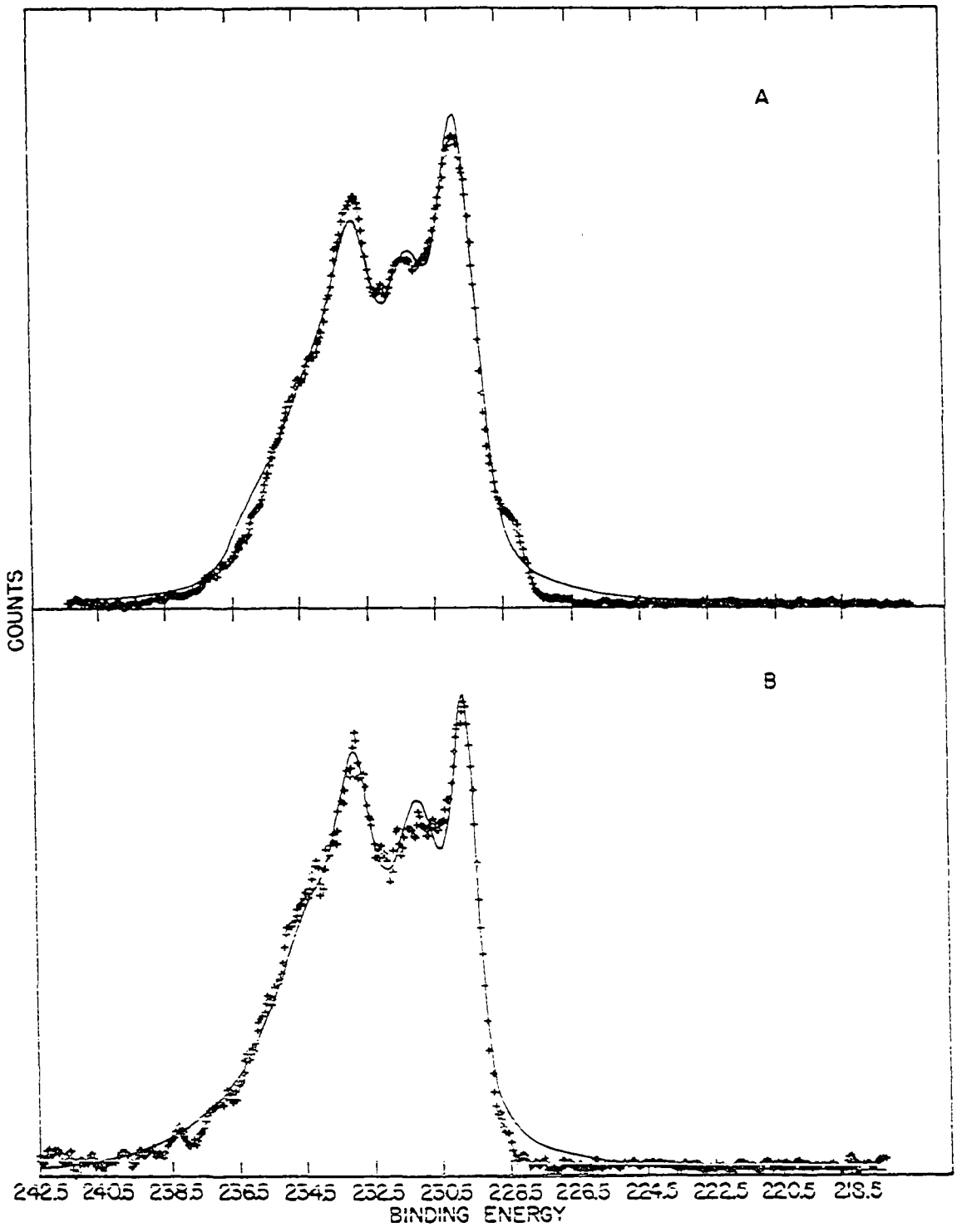

Figure 5. XPS data for $H_{1.7}MoO_3$ prepared by a) the "wet" preparation method and b) dry hydrogen spillover

Table II. XPS data for bronzes[a]

$H_{1.66}MoO_3$ (hydrogen spillover)		Mo Type I	Mo Type II	Mo Type III
Binding Energy (eV)	Mo $3d_{\frac{5}{2}}$	229.7	231.0	233.1
	$3d_{\frac{3}{2}}$	232.9	234.3	236.3
FWHM (eV)		1.0 ± 0.2	2.3 ± 0.4	3.7 ± 0.6
$H_{1.74}MoO_3$ ("wet" preparation)				
Binding Energy (eV)	Mo $3d_{\frac{5}{2}}$	229.8	231.2	232.7
	$3d_{\frac{3}{2}}$	233.0	234.4	235.9
FWHM (eV)		1.5 ± 0.2	1.9 ± 0.3	1.5 ± 0.3

[a]Binding energies are referenced to C at 285.0 eV.

The assignments of type II as predominantly Mo^{+5} and type III as predominantly Mo^{+6} do not seem to be unreasonable. The difficulty in interpreting the spectra lies in the rather broad FWHM for that portion of the spectra associated with Mo^{+5} and Mo^{+6}. These somewhat broad structureless features preclude an unambiguous determination of the number of the different types of Mo present, assuming the model of three types of Mo.

For the purpose of the present discussion, the most important point of Figure 5 is that the spectra of both samples are essentially identical.

Table III. Binding energy values for Mo 3d doublet

SAMPLE	REFERENCES[a,b]	BINDING ENERGY (eV)		FWHM[c] (eV)
		$3d_{\frac{5}{2}}$	$3d_{\frac{3}{2}}$	
Mo	110	228.0	231.2	1.3 ± 0.2
MoO_2	110	229.3	232.4	1.6 ± 0.2
	111	229.5	232.7	
MoO_x[d]	110	231.2	234.3	2.1 ± 0.2
(Mo^{+5})	111	231.8-231.3	235-234.8	
MoO_3	110	232.3	234.4	1.4 ± 0.2
	111	232.8	236	

[a]Mo metal binding energies from Reference 110 agree with those used for Table I. The data may be directly compared.

[b]The values reported in this table from Reference 111 were adjusted to make C = 285.0 eV to allow direct comparison with Table II.

[c]Full width at half maximum.

[d]$2 < x < 3$.

The similarity of the two samples is also seen in the response of the protons in these samples to a single pulse NMR experiment at room temperature. The bronzes show an effective transverse relaxation time, T_2^*, of approximately 3 msec. This relaxation time, which is unusually long for protons in solids, can be explained in terms of motional averaging of static homonuclear

dipolar interactions. That such motional averaging takes place is indicated by a comparison of the hydrogen NMR absorption spectra of the spillover bronze under a single pulse experiment (Figure 6(a)) and that from an experiment which removes static interproton dipolar interactions by strong pulse decoupling (Figure 6(b)). Both the lineshape and the magnitude of the anisotropy of the Fourier transform of the Free Induction Decay (FID), as shown in Figure 6(a), are characteristic of anisotropic magnetic shielding. The fitted spectra indicate the shielding to be axially symmetric, with an anisotropy of $\Delta\sigma = \sigma_{\parallel} - \sigma_{\perp} = -22.7$ ppm and an isotropic value of -3.6 ppm relative to H_2O. The same lineshape and anisotropy are obtained under the MREV-8 multiple pulse sequence (40, 41, 44), as shown in Figure 6(b), which has been shown to remove static homonuclear dipolar broadening to first order, when the frequency scaling under the MREV-8 sequence is taken into account. The important point is that the particular motion responsible for averaging the homonuclear dipolar interactions does not average the shielding anisotropy in this sample. This effect is easily understood when it is realized that the shielding is tied to the lattice, but the proton-proton internuclear vectors are determined by proton hopping.

Figure 7 shows the Fourier transform of the FID for the "wet" preparation bronze at room temperature. There is found

Figure 6. ^{1}H NMR absorption spectra for the hydrogen spillover bronze under a) a single pulse experiment and b) a homonuclear decoupling experiment

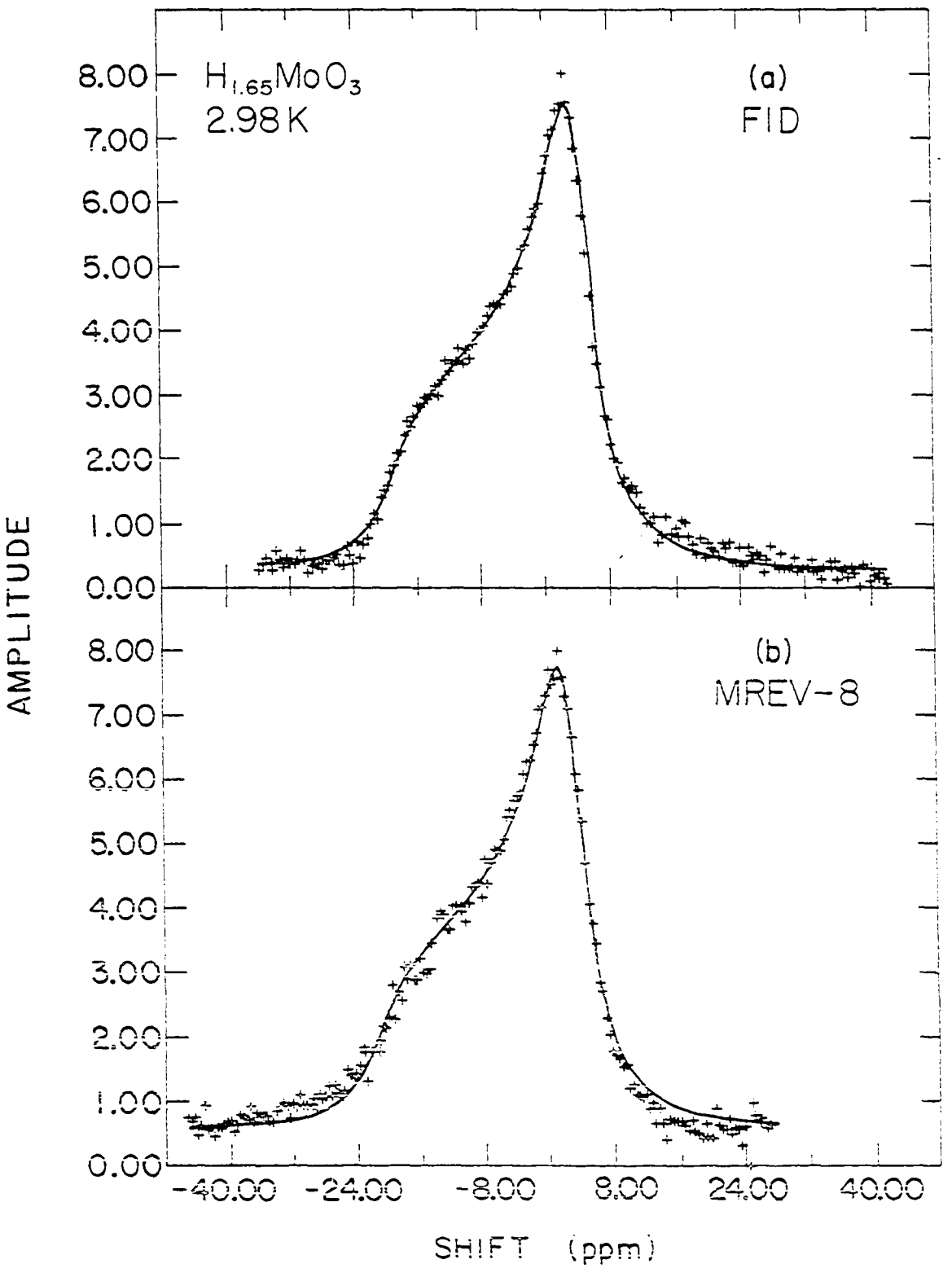
$H_{1.65}MoO_3$
2.98 K
(a)
FID
(b)
MREV-8
AMPLITUDE
SHIFT (ppm)
8.00
7.00
6.00
5.00
4.00
3.00
2.00
1.00
0.00
-40.00
-24.00
-8.00
8.00
24.00
40.00

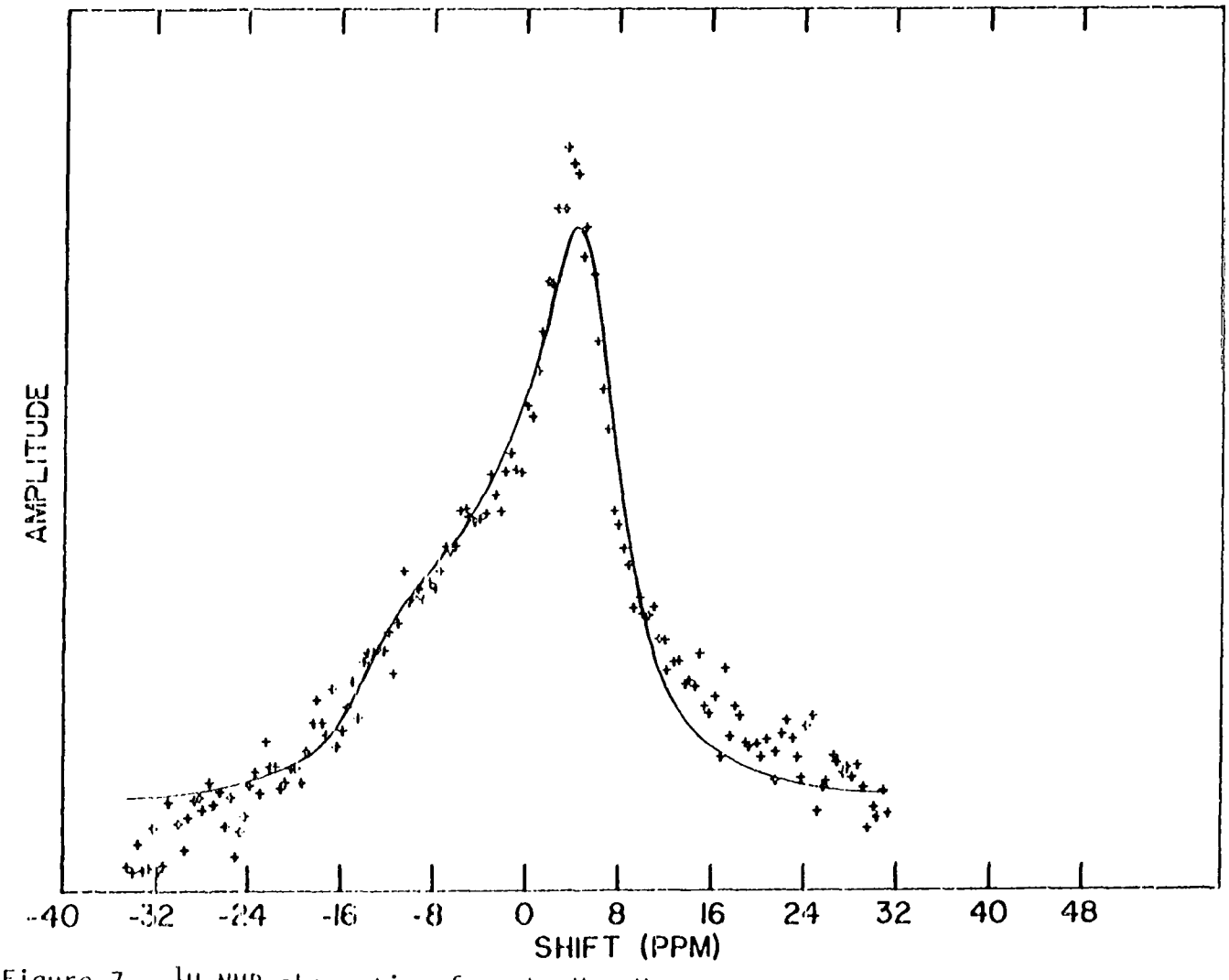

Figure 7. ^{1}H NMR absorption for the "wet" preparation bronze under a single pulse experiment

an anisotropy of $\Delta\sigma$ = -20.3 ppm with an isotropic value of -1.0 ppm with respect to H_2O. The anisotropies of the two bronzes overlap within experimental error, assuming an uncertainty of ±1 ppm for any tensor component. However, it is interesting to note that Slade et al. (66) reported an anisotropy of $\Delta\sigma$ = -20.1 ppm for $H_{1.71}MoO_3$ made by the "wet" method. For comparison the values of the shielding tensors are given in Table IV.

Magic angle spinning (MAS) can be used to remove the shielding anisotropy (23-29). The NMR spectrum of ^1H for the hydrogen spillover bronze under MAS is shown in Figure 8(a). The major species is at -3.6 ppm relative to water. A second species of proton (2% of the total proton concentration) is found upfield at +5 ppm. The two peaks at +15 and -23 ppm are spinning sidebands. In the "wet" preparation bronze (Figure 8(b)), the concentration of the second species is 12% (±2%). (In the NMR spectra, corrections for magnetic susceptibility (61) [$\chi \sim 2 \times 10^{-7}$emu cgs/g] were neglected.)

Under MAS, the FWHM is 1.96 ppm for the hydrogen spillover bronze and 2.64 ppm for the "wet" preparation bronze. A discussion of the resolution achievable with the present spectrometer has been given by Ryan et al. (103). However, for the present purpose, a liquid H_2O sample in a rotor (nonspinning) with signal averaging has a FWHM of 0.6 ppm.

Table IV. ^1H shielding tensors for $H_{1.7}MoO_3$[a]

SAMPLE	$\sigma_{\parallel}$	$\sigma_{\perp}$	σ_{iso}[b]	$\Delta\sigma$[c]
$H_{1.66}MoO_3$ (hydrogen spillover)	-18.7	3.9	-3.6	-22.7
$H_{1.74}MoO_3$ ("wet" preparation)	-14.6	5.7	-1.0	-20.3

[a] Reference is in ppm relative to H_2O.

[b] $\sigma_{iso} = \frac{1}{3}(2\sigma_{\perp} + \sigma_{\parallel})$.

[c] $\Delta\sigma = (\sigma_{\parallel} - \sigma_{\perp})$.

The maximum error in setting the magic angle (105) is less than 0.5 degree, introducing an error of less than 0.25 ppm. T_1 has been measured to be 125 msec at room temperature. Lifetime broadening under a single pulse experiment is $\frac{1}{\pi T_1} = 0.05$ ppm. Thus, the observed linewidth is not limited by experimental conditions or lifetime broadening. However, one should note that the same asymmetry of the predominant species is observed in both samples. A crystal of MoO_3 (69) consists of distorted octahedra, with each octahedron sharing two adjacent edges with its neighbors to form zig-zig chains. The asymmetry may result from a shielding dispersion due to different oxygen atoms having different numbers of Mo nearest neighbors. Still, the achievable resolution indicates at least two distinctly different proton species.

Figure 8. ^{1}H NMR absorption spectra of hydrogen spillover bronze (a) and the "wet" preparation bronze (b) under magic angle spinning

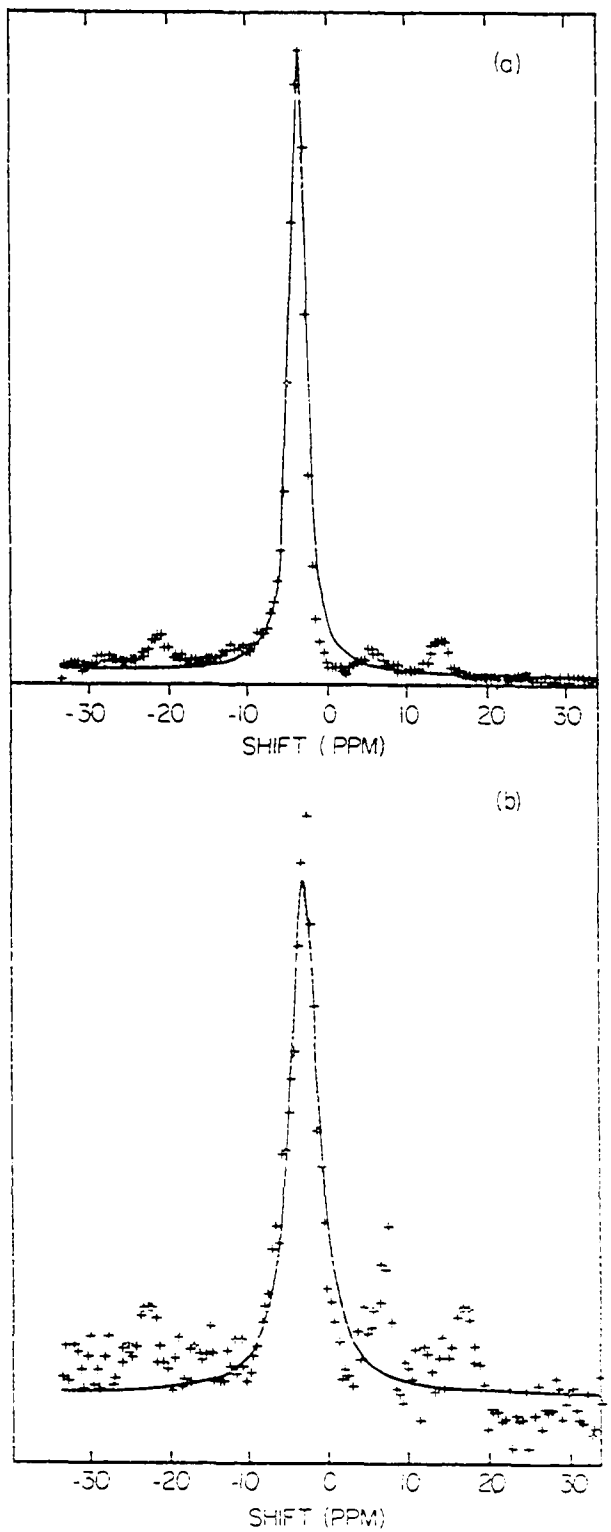
(a)
-30
-20
-10
0
10
20
30
SHIFT (PPM)
(b)
-30
-20
-10
0
10
20
30
SHIFT (PPM)

The high field species may be a hydride associated with Mo. Although Mo is not generally thought of as a hydride former, the species MoH has been reported (112).

The identification of the low field species proves more difficult. Figure 9 shows the ^1H NMR spectra of the bronze prepared by hydrogen spillover under sample rotation at various angles with respect to the magnetic field. The solid lines show a computer fit of the analytical expression for a shielding tensor under rapid sample rotation given by equation 38 fitted under the assumption that only one species is present. Under all spinning angles except at the magic angle, the observed lineshape near the center of the spectrum can be reasonably well-described by the assumption of one magnetic shielding tensor. The presence of the minor species (2% of the total proton concentration) is probably the cause of the poor fit in the wings (ignoring the obvious artifact of the two spinning sidebands at the outside of all spectra). If the observed lineshape is due to the predominant species of proton, then it should be noted that the anisotropy of -22.7 ppm, although of similar magnitude, is <u>opposite</u> in sign to that of hydrogen-bonded -OH groups, for example, in ice (113, 114).

However, the absence of static homonuclear dipolar broadening, as inferred from Figure 6, indicates proton motion. Indeed, the proton motion is reflected in both the spin-lattice (Figure 10)

Figure 9. ^{1}H NMR absorption spectra of the hydrogen spillover bronze under sample rotation at various angles with respect to the magnetic field

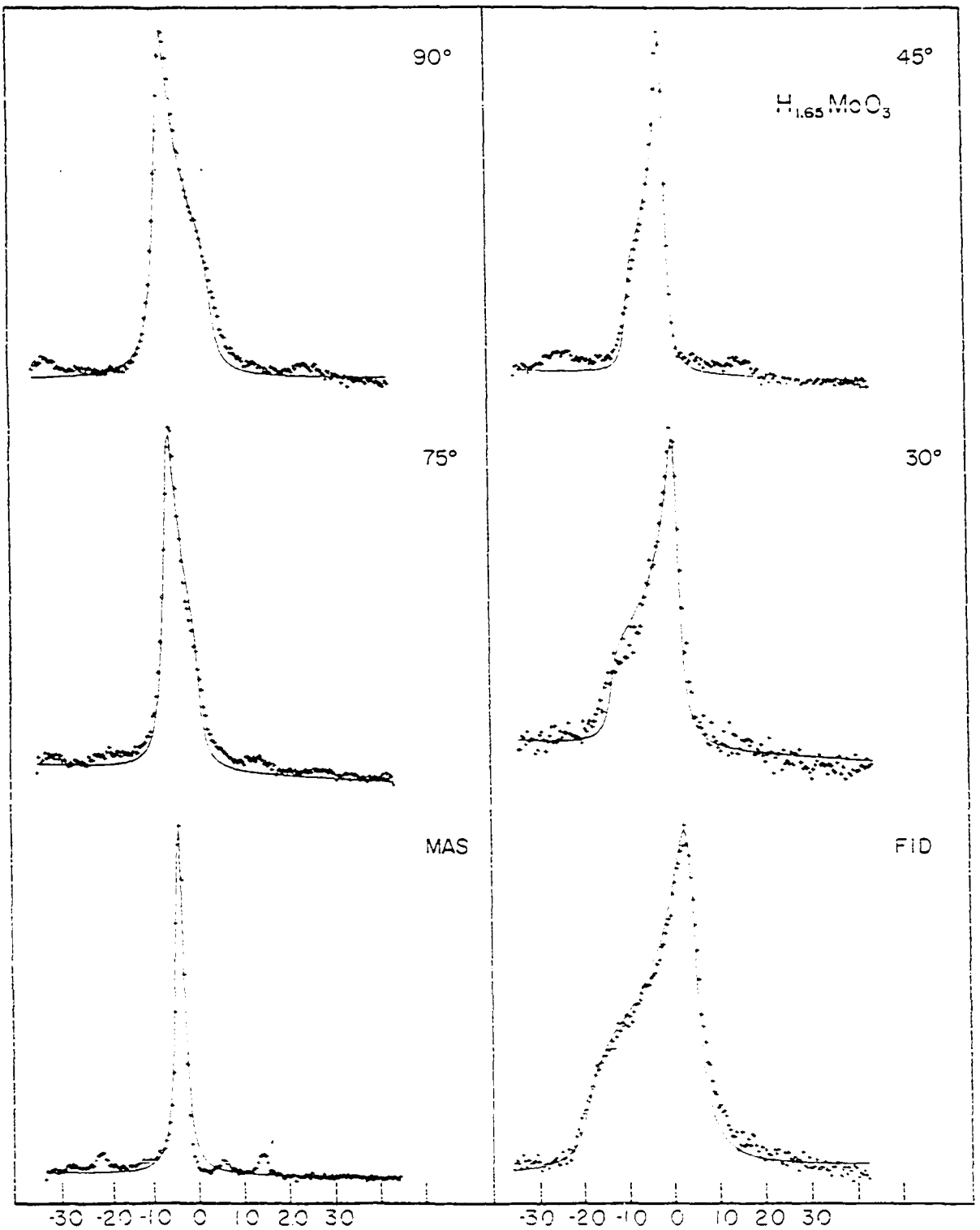
90°
45°
$H_{1.65}MoO_3$
75°
30°
MAS
FID
-30 -20 -10 0 10 20 30
-30 -20 -10 0 10 20 30

Figure 10. Temperature dependence of the spin-lattice relaxation time at 56 MHz. The value of $(T_{1e}T)$ in sec K is obtained from the slope of the line

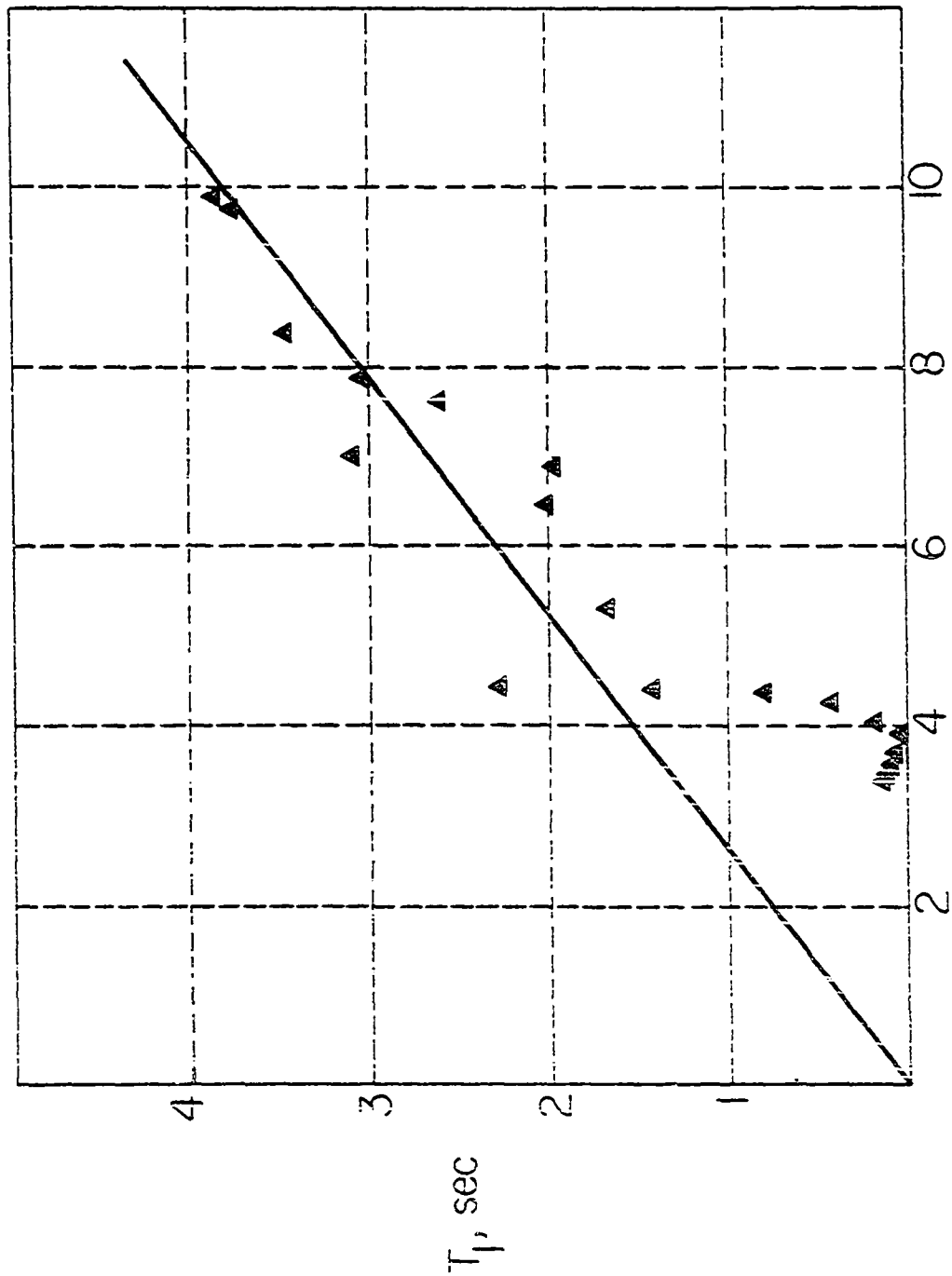
4
3
2
1
T_1, sec
2
4
6
8
10
$\frac{1}{T} \times 10^3$, K^{-1}

and the spin-spin (Figure 11) relaxation times as a function of temperature. The spin-lattice relaxation time may be analyzed according to BPP (17) theory with

$$\frac{1}{T_1} = C_1\left[\frac{\omega\tau}{1 + \omega^2\tau^2} + \frac{2\omega\tau}{1 + 4\omega^2\tau^2}\right]. \qquad (40)$$

The minimum for T_1 occurs at $\omega\tau = \frac{1}{\sqrt{2}}$, so the constant C_1 is given by

$$C_1 = \frac{3}{2^{2/3}}\left(\frac{1}{T_{1\min}}\right). \qquad (41)$$

Correcting the observed spin-lattice relaxation times for the contribution from the conduction band electrons ($T_{1e}T$ = 300 sec K), the spin-lattice relaxation times, resulting from homonuclear dipolar interactions, gave a correlation time of 1.7×10^{-9} sec at 295 K with an activation energy of E_a = 0.4 eV. These values are in reasonable agreement with the correlation time of $\sim 6 \times 10^{-9}$ sec and activation energy of E_a = 0.3 eV obtained by Cirillo and Fripiat (59). Cirillo et al. (60) estimated a diffusion coefficient from the spin-lattice relaxation times of the protons on the order of 4×10^{-7} cm^2/sec.

In an effort to learn more about the mobility of the protons, the diffusion coefficient was measured by the pulsed field gradient technique of Stejskal and Tanner (88). The measurement of proton diffusion within the bulk of the hydrogen spillover bronze 298 K is facilitated by the absence of static homonuclear dipolar interactions. The hydrogen spillover sample was chosen since it has essentially one proton species

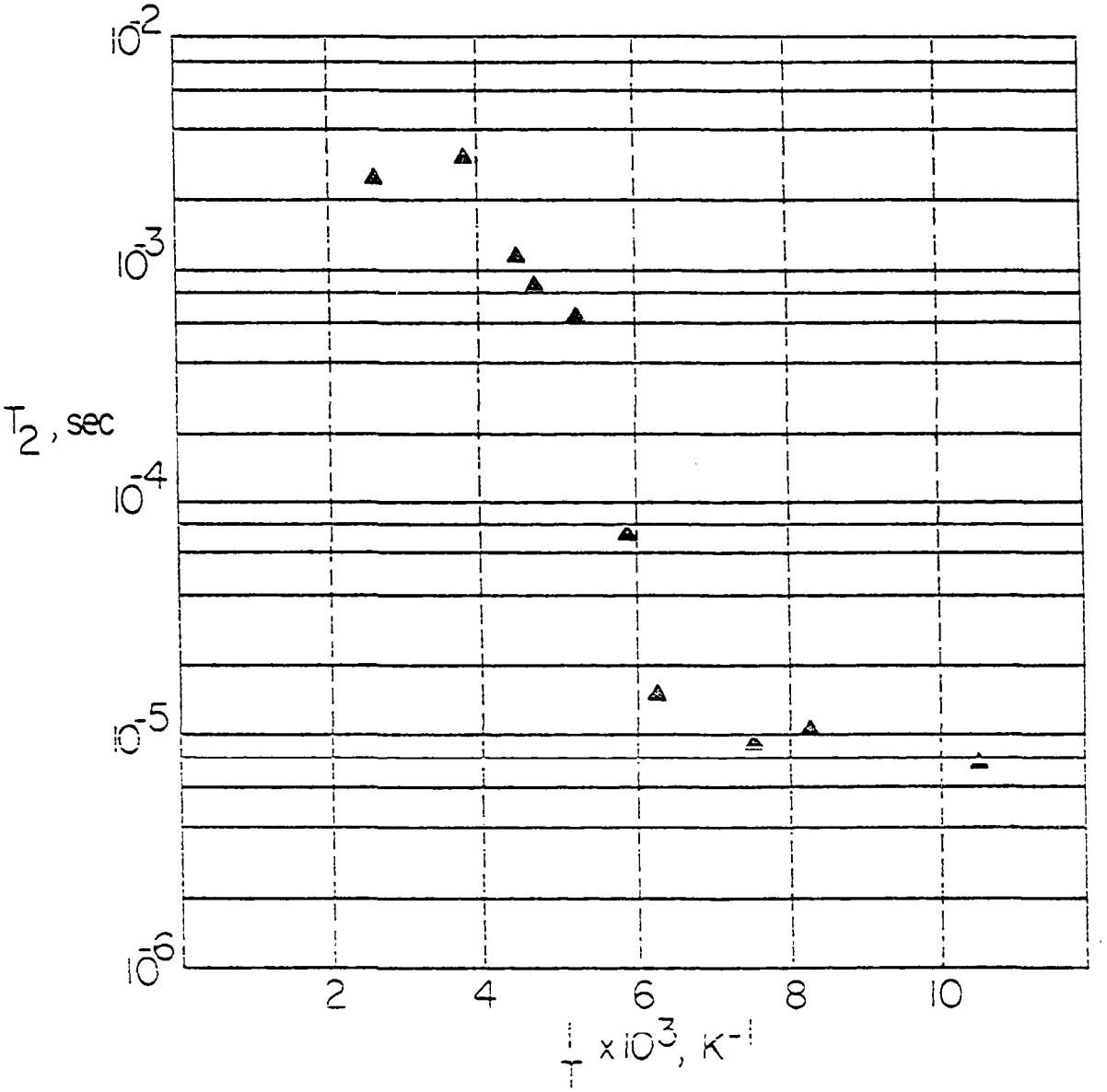

Figure 11. Temperature dependence of the spin-spin relaxation time

(98% of the total proton concentration). The background gradient of $H_{1.65}MoO_3$ was estimated to be $G_o \sim 15$ gauss/cm by the comparison of a single spin echo amplitude to the echo amplitude under the Carr-Purcell sequence, as discussed in the Basic Theory section. Using an applied field gradient of $G \sim 300$ gauss/cm to meet the condition of $G >> G_o$, a proton diffusion coefficient of $D = (7.9 \pm 1.6) \times 10^{-6}$ cm^2/sec was obtained for $H_{1.65}MoO_3$ by varying δ. The results are shown in Figure 12. The standard used for this diffusion experiment was H_2O. In order to determine the effect upon the measured value of the diffusion coefficient by eddy currents induced by the applied gradient within the sample, the experiment was repeated by applying a constant gradient G for a constant time δ, such that any induced background would be constant. The diffusion coefficient was obtained by varying only Δ, the time between gradients. Within experimental error, the same value of D was obtained.

Since the value of the diffusion coefficient obtained from the spin-lattice relaxation times was calculated with the assumption of isotropic motion, the difference between the calculated diffusion coefficient and the experimentally measured one may give an indication of the degree of anisotropy in the proton motion within the bronze. (It should be pointed out that artifacts of the pulsed gradient experiment are such that errors in the experiment would cause the experimentally measured value

Figure 12. ^{1}H translational self-diffusion coefficient for $H_{1.65}MoO_3$ at 298K

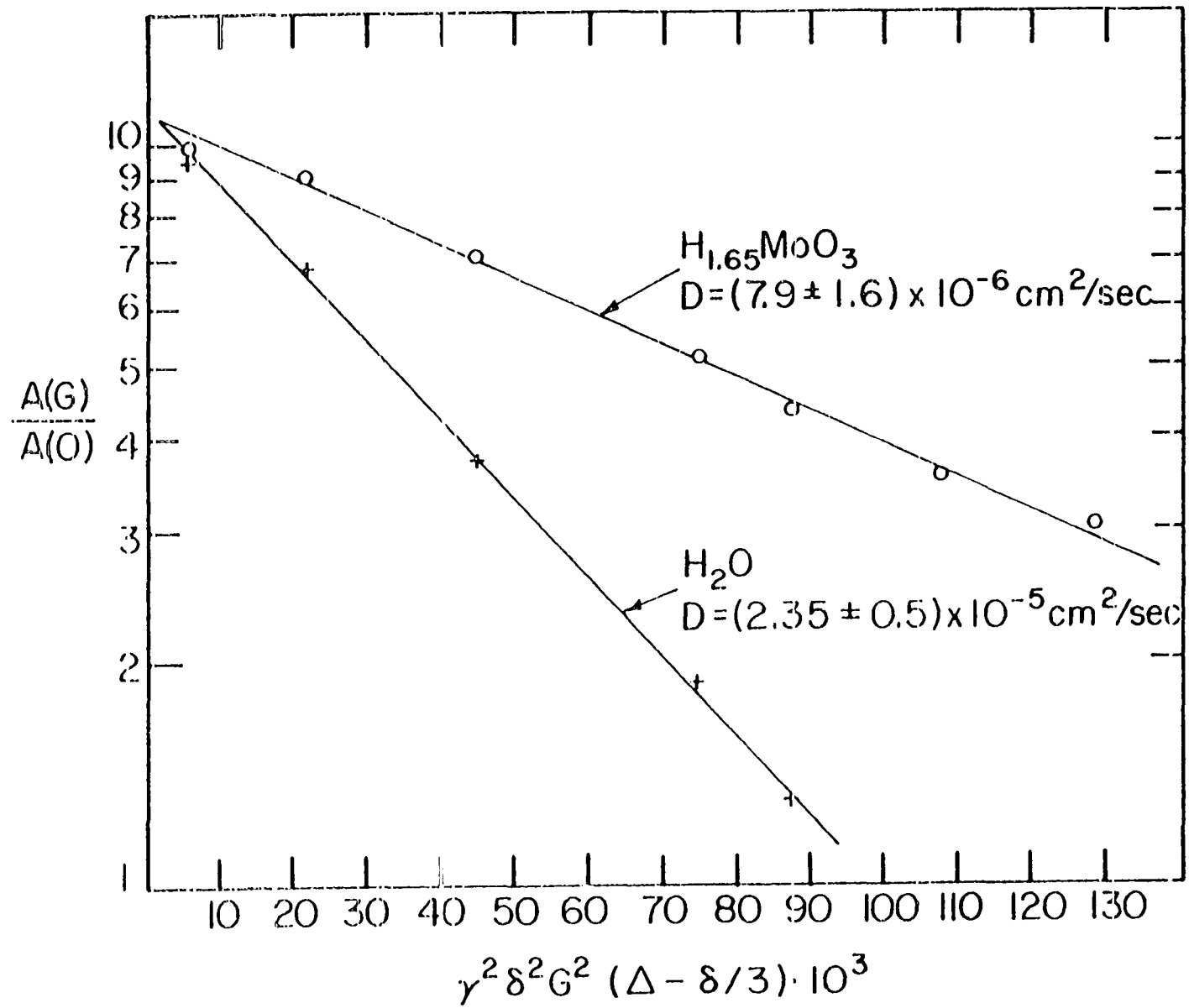
A(G)/A(0)
10
9
8
7
6
5
4
3
2
1
$H_{1.65}MoO_3$
$D=(7.9\pm1.6)\times10^{-6}cm^2/sec$
H_2O
$D=(2.35\pm0.5)\times10^{-5}cm^2/sec$
10 20 30 40 50 60 70 80 90 100 110 120 130
$\gamma^2\delta^2G^2(\Delta-\delta/3)\cdot10^3$

to be larger than the actual value. The repetition of the experiment with a constant gradient was an effort to show that the measured value is indeed the actual value.) It should also be noted that a high temperature (~300 K) plateau (Figure 11) in the effective spin-spin relaxation times has been observed (66) and may also be a reflection of anisotropic diffusion. If this is the case, the observed shielding powder pattern under a single pulse experiment may be the result of averaging by rapid anisotropic motion. The effect of anisotropic molecular reorientation on the shielding tensor is well-known (13). The value of $\Delta\sigma$, -22.7 ppm, observed for the bronze at room temperature (in comparison to $\Delta\sigma$ = 28.7 ppm for ^1H in polycrystalline ice (114)) clearly negates an identification of this species as a proton rotating about the C_2 axis at a speed fast compared to the anisotropy of the shielding tensor of hydrogen in ice.

In order to learn more about the nature of the predominant species of proton, low temperature NMR studies were performed. Under a single pulse experiment, the difference bewteen the two bronzes becomes more evident. Figure 13 shows the ^1H NMR absorption under a single pulse experiment at 90 K for both the hydrogen spillover (A) and "wet" preparation (B) bronzes. Instead of the usual broad featureless spectra found in most rigid solids, both bronzes display structure in the dipolar spectra. The difference between the spectra is clearly evident.

Figure 13. ^1H NMR spectra under a single pulse excitation at 90 K for the hydrogen spillover bronze (A) and the "wet" preparation bronze (B)

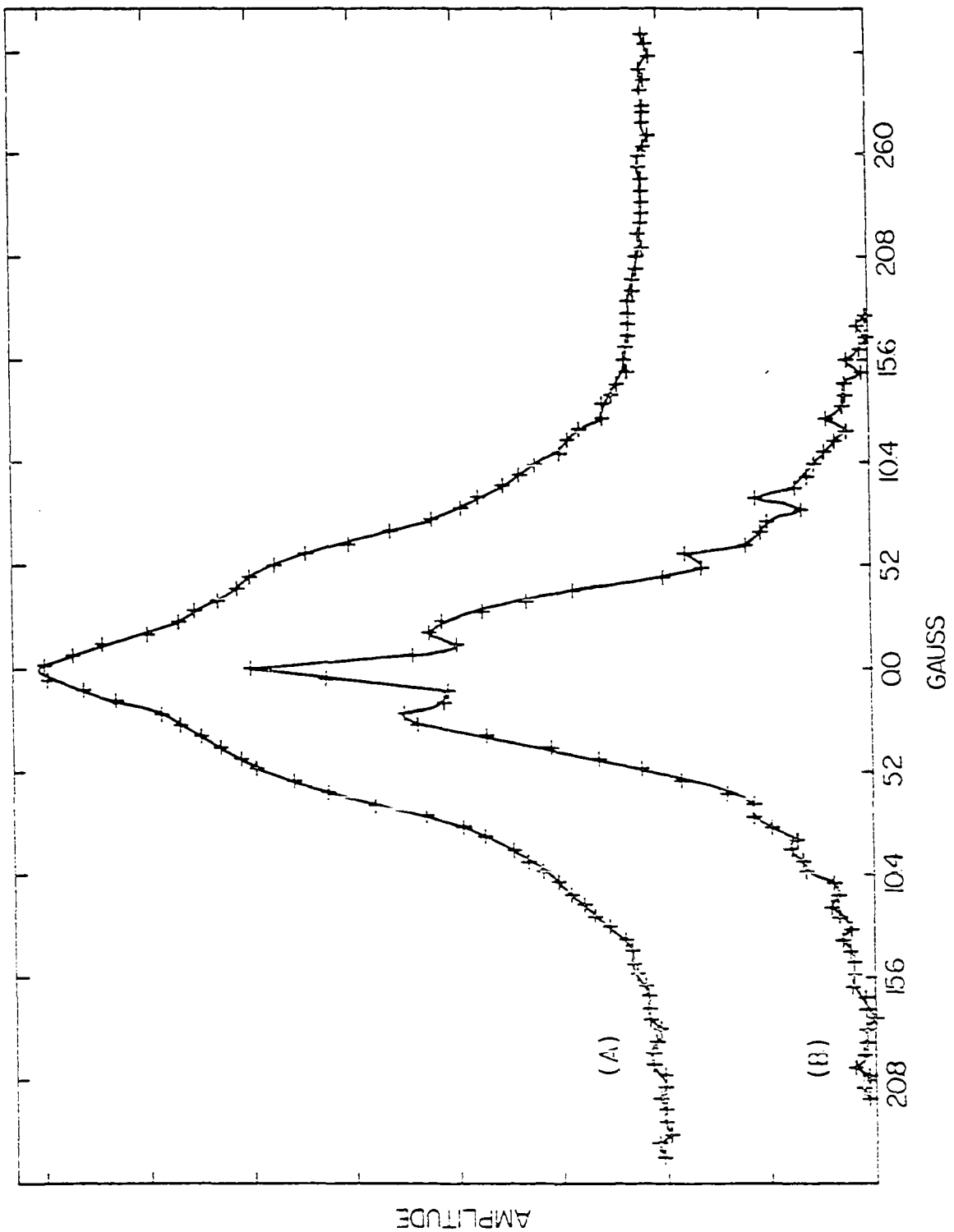
AMPLITUDE
(A)
(B)
208
156
104
52
00
52
104
156
208
260
GAUSS

Figure 14 shows the ^1H NMR absorption spectrum for the hydrogen spillover bronze under a multiple pulse homonuclear decoupling experiment using the Burum and Rhim 24 pulse sequence (43) at 90 K. The solid line shows a computer fit of a shielding tensor (under the assumption that the high field species contributes negligibly to the signal) with the same anisotropy as was observed at room temperature but with a larger broadening function. The residual broadening presents problems in determining the exact anisotropy. Since the multiple pulse sequence has been used to average the static homonuclear dipolar broadening for protons in ice (43), certainly one of the most severe tests of the narrowing ability of the sequence, the residual broadening could be heteronuclear in origin, resulting from the dipolar coupling of the protons to the quadrupolar species of Mo. A dipolar narrowed Carr-Purcell experiment (48), which averages homonuclear dipolar interactions, magnetic shielding anisotropy, magnetic shielding, and heteronuclear dipolar broadening, at 90 K gives a time constant of $T_{1y} = 25.4$ msec. This number corresponds to a Lorentzian linewidth of $\frac{1}{\pi T_{1y}} = 12.5$ Hz, demonstrating that the linewidth observed under homonuclear decoupling experiments at 90 K is shielding and heteronuclear broadening.

Spin-lattice (T_1) relaxation times were also recorded (Figure 10) down to 85 K using an inversion recovery technique in order to obtain a better value (59) of $T_{1e}T$. The value of

Figure 14. ^{1}H NMR absorption spectrum for the hydrogen spillover bronze under a multiple pulse homonuclear decoupling experiment at 90 K

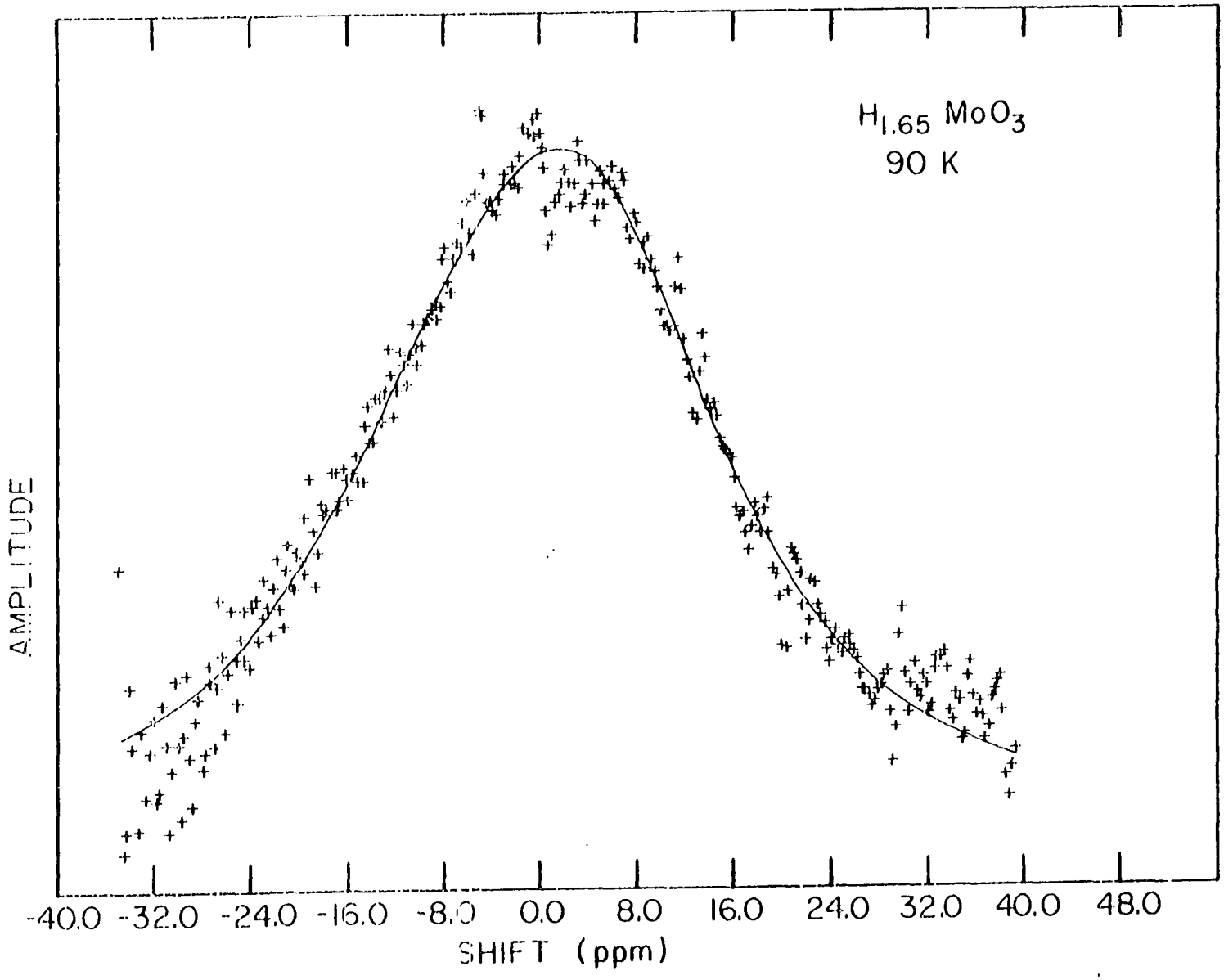
$H_{1.65}\ MoO_3$
90 K
AMPLITUDE
-40.0 -32.0 -24.0 -16.0 -8.0 0.0 8.0 16.0 24.0 32.0 40.0 48.0
SHIFT (ppm)

$T_{1e}T$ = 300 sec K is in the range of that found for protons in metallic hydrides. For example, protons in $YH_{1.92}$ (81) have $T_{1e}T$ = 286 sec K. The usual expression for the T_1 relaxation due to conduction electrons is given by (31)

$$\frac{1}{T_{1e}} = \frac{64}{9}\pi^3\hbar^3\gamma_e^2\gamma_n^2 k_B T \langle|\Psi(0)|^2\rangle_{E_F}^2 \rho^2(E_F), \tag{40}$$

where γ_e represents the gyromagnetic ratio for electrons, γ_n represents the gyromagnetic ration for nuclei, k_B is Boltzmann's constant, and $\rho(E_F)$ is the density of states at the Fermi surface. The quantity ξ can be defined as

$$\xi = \frac{\langle|\Psi(0)|^2\rangle_{E_F}}{\langle|\Psi(0)|^2\rangle_{atom}}, \tag{41}$$

where $\langle|\Psi(0)|^2\rangle_{atom}$ is the electron density at the proton site for a free hydrogen atom and $\langle|\Psi(0)|^2\rangle_{E_F}$ is the corresponding contribution from conduction electrons obtained from an average over all orbits at the top of the Fermi distribution. The rate expression for $\frac{1}{T_{1e}}$ is the result of the contact interaction with the S-like conduction electrons which is appropriate for hydrogen since the 1S part of the conduction electron wavefunction is expected to be the important part for the proton. So, ξ is a measure of the conduction band electron density near the proton. Making the same approximations as Schreiber (115) yields a value of $\xi \sim 0.37$, confirming a significant portion of the hydrogen electrons are in the conduction band of $H_{1.7}MoO_3$.

However, one must exercise caution in using low temperature data to explain room temperature phenomena. Both a discontinuity in the heat capacity (62) and a change in the susceptibility behavior (61) from Pauli-type at high temperatures (300 - 220 K) to Curie behavior below 220 K have been observed in $H_{1.65}MoO_3$.

Dickens et al. (64) used results from inelastic neutron scattering at 80 K to infer the presence of $-OH_2$ groups in the bronze. Neither this work nor that of Cirillo et al. (60) discounts the existence of an associated pair at low temperatures. However, the room temperature proton NMR data is not consistent with this model. The shielding tensor and proton mobility in $H_{1.7}MoO_3$ at room temperature suggest the predominant, low field proton species to be a unique entity.

Debate exists over the nature of the protons in the hydrogen molybdenum bronzes, with these compounds also having been formulated as oxyhydroxides, $MoO_{3-x}(OH)_x$ (71). The present work indicates this not to be an appropriate formulation. There are two chemical species of protons in these materials. At room temperature, there is also evidence to indicate that the dominant species is not a hydroxyl proton. Although the data at lower temperatures does not preclude the existence of an associated pair such as $-OH_2$, the low temperature spin-lattice relaxation data indicates a behavior similar to that of metallic hydrides, as pointed out by Cirillo and Fripiat (59).

In fact, while many physical properties are alike, the two hydrogen molybdenum bronze samples used in this study were not identical, as evidenced by the low temperature proton NMR spectra under single pulse excitation. In addition, the bronze prepared by the "wet" method contained a greater concentration of the high field species of proton relative to the predominant species. Hence, the method of preparation proves to be an important point.

With regards to the method of preparation, the measurement of the proton diffusion in the hydrogen spillover bronze provides information about the rate determining step for the formation of $H_{1.7}MoO_3$ via hydrogen spillover. The formation of $H_{1.7}MoO_3$ by hydrogen spillover has been described by Cirillo and Fripiat (59) as occurring in three steps: first, dissociative chemisorption of molecular hydrogen on the surface of the platinum; second, transfer of the hydrogen species formed to the oxide; and third, reduction of the oxide lattice. Levy and Boudart (116) have shown water to be an efficient carrier for the second step. Cirillo and Fripiat noted that even when working with dry hydrogen gas it can be assumed that surface hydration produces a small amount of water which could act as a carrier. However, the absence of water from the sample has been confirmed by ^1H NMR using magic angle spinning, as shown in Figure 8(a).

Sermon and Bond (70) have calculated the maximum rates and diffusion coefficients for the hydrogen spillover process

Table V. Diffusion coefficients for bronzes

System	Diffusion Coefficient
	Hydrogen Spillover, $D/10^{-16} cm^2/sec$
Pt/WO_3	1.7[a]
Pt/MoO_3	1670.[a]
	^1H Self-diffusion, $D/10^{-6} cm^2/sec$
H_xWO_3	7.[b]
$H_{1.7}MoO_3$	7.9[c]

[a]Ref. 70.

[b]Ref. 117.

[c]This work.

in Pt/WO_3 and Pt/MoO_3. These results are shown in Table V. It should be noted that the maximum diffusion coefficient for Pt/MoO_3 is approximately a thousand times larger than that obtained for Pt/WO_3. These data show that the ^1H self-diffusion within the bulk is 10^7 and 10^{10} times greater than that calculated for the overall spillover process in Pt/MoO_3 and Pt/WO_3, respectively. This clearly eliminates diffusion in the bulk of the bronze from being the rate limiting step in the formation of the bonze.

In the overall reduction process, the following steps may be proposed to occur in series:

(1) Transport of molecular H_2 to the Pt surface;

(2) Dissociation of the hydrogen on the Pt;

(3) Diffusion of atomic hydrogen through the MoO_3 surface; if surface hydration is assumed to produce a small amount of water to act as a carrier, then

(3a) diffusion of atomic hydrogen through an H_2O monolayer to the MoO_3 surface and

(3b) transfer across the H_2O-MoO_3 interface;

(4) Diffusion of hydrogen through the MoO_3.

Information about the rate determining step can be obtained from Table VI.

The large values of the diffusion coefficients from Table VI preclude steps 1 and 4 from being rate determining. For the case of sufficient (monolayer) surface hydration, step 3a may also be ruled out. Cirillo (14) has prepared sample of the hydrogen molybdenum bronze with 0.25%, 0.50%, and 2.0% Pt by weight. The kinetics of the reaction were independent of the number of platinum particles, which rules out step 2. The rate limiting step appears to be the diffusion of atomic hydrogen through the MoO_3 surface.

In studying H_xWO_3, Vannice et al. (77) presented strong evidence to suggest that the rate determining step in the reduction is the penetration of the reducing species below the surface of the WO_3 particles. Levy and Boudart (116) confirmed that the release of the proton from the carrier with interfacial

Table VI. Diffusion coefficients for various species

System	D(cm^2/sec)	Reference
H_2 (gas, 1 atm., 80°C)	1.7	117
Molecular H_2 in H_2O	3.4×10^{-5}	77
Atomic H in H_2O	7×10^{-5}	118
Protons in a H_2O Monolayer	10^{-8}	119
Hydrated electrons in H_2O	4.8×10^{-5}	120
Hydrogen in MoO_3	7.9×10^{-6}	This work

crossing is rate determining in the presence of sufficient carrier. However, they noted a dependence of the rate on the amount of absorbed carrier below monolayer coverage. In the present study, it is impossible to unambiguously determine the rate determining step since the rate of reaction may be limited by the amount of surface hydration. Still, in the presence of sufficient carrier (or possibly for the case of intimate contact between the Pt and MoO_3 particles), the rate determining step in such a process in the formation of $H_{1.7}MoO_3$ is the penetration of spilled over hydrogen through the surface of MoO_3.

High Resolution Proton NMR of $YH_{1.92}$

Accurate second moments are needed to determine the fractional occupation of octahedral and tetrahedral sites in metallic

hydrides. Since theoretical second moments are calculated assuming dipolar interactions, it would appear to be useful to quantify the magnitude of other interactions present and their contributions to the experimental second moment.

Free induction decays were obtained at 323, 296, and 86 K. Full widths at half-height (2δf) were 15.9, 34.2, and 41.6 KHz, respectively. A previous wideline ^1H NMR study (121) has shown that the onset of thermal line narrowing occurs around room temperature. Fitting the room temperature FID's to Lorentzian and Gaussian decays gave T_2 = 10.6 usec ($\frac{1}{\pi T_2}$ = 29.5 kHz) and T_2 = 16.9 usec ($\frac{[2\ln 2]^{\frac{1}{2}}}{\pi T_2}$ = 22.1 kHz), respectively. A more satisfactory fit of the lineshape was obtained by using the Harper-Barnes lineshape (122), which has the analytical form

$$g(x) = A \exp(-b|x|^n) \qquad (42)$$

where $x = \nu - \nu_o$. Since a determination of n readily gives the second moment, this allows a judgment of goodness of fit bypassing the usual difficulty of establishing the proper baseline for the measurement of second moments. At room temperature, the exponent n was 2.1. However, at 86 K the best fit was given by n = 2.8. Increases in n, leading to a more rectangular shape than a Gaussian, at lower temperatures have been observed in other metallic hydrides (123). The second moment obtained from the fit of the Harper-Barnes lineshape to the 86 K FID was 11.17 gauss^2. This may be compared to the

value of 10.68 (±0.26) gauss^2 obtained by direct numerical integration of cw derivative recordings (80).

Homonuclear decoupling experiments gave symmetric lineshapes with $2\delta f \sim 2.9$ kHz at 323, 296, and 86 K. Fitting the 86 K data with the Harper-Barnes lineshape gave a second moment of 0.16 gauss^2, which is smaller than the standard deviation in the second moment reported by Anderson et al. (80). The combined homonuclear decoupling and magic angle spinning experiments at room temperature gave a proton Knight shift of K_H = -5.9 (±1.6) ppm [σ = +5.9 ppm] with respect to H_2O. The linewidth was $2\delta f \sim 525$ Hz. A phase-altered MREV-8 sequence $[P_x - M_y]$ (47), which removes inhomogeneous magnetic broadening, gave a linewidth of $2\delta f \sim 415$ Hz at 86 K.

The measurement of the second moment under the homonuclear dipolar decoupling experiment allows the determination of the contribution from the shielding anisotropy, higher order homonuclear dipolar broadening, heteronuclear dipolar broadening, etc. For $YH_{1.92}$, the correction to the experimental second moment from other mechanisms of line broadening is within the observed standard deviation. At 56 MHz, the ratio of the second moment under the homonuclear decoupling experiment to the second moment of the FID is $\frac{M_2(\text{MREV-8})}{M_2(\text{FID})}$ = 1.5%. When the second moments are measured at lower fields, the correction may even be smaller if there is any field dependence.

The homonuclear decoupling experiment gives a symmetric lineshape with $2\delta f \sim 2.9$ kHz. If the protons reside at the center of the tetrahedral and octahedral sites which have cubic symmetry, there should be no shielding anisotropy. The phase-altered sequence which suppresses both homonuclear dipolar interactions and interactions which go as I_z, such as anisotropic shielding and heteronuclear dipolar broadening, significantly narrows the line to ~ 0.4 kHz. The difference between these two experiments gives a value of ~ 2.5 kHz, which is probably due to heteronuclear dipolar broadening. The inability of the multiple pulse sequences to completely narrow the line is easily explained in terms of the correlation time obtained from the change in linewidth at the onset of thermal line averaging. Anderson (121) has found a correlation time of ~ 10 usec at room temperature. This correlation time is of the same order of magnitude as the multiple pulse cycle times presently achievable and limits the ability of the multiple pulse sequence to narrow.

Schreiber (124) has modified the Korringa relation by the introduction of a parameter ρ according to

$$K^2(T_{1e}T) = \rho^2 S \qquad (43)$$

where $S \equiv (\gamma_e/\gamma_n)^2(\frac{\hbar}{4\pi k_B})$. The intrinsic Knight shift relative to bare protons is given by

$$K_H = K_H(\text{observed}) - 25.6 \text{ (in ppm)}, \qquad (44)$$

where the molecular shielding constant of protons in water is taken to be 25.6 ppm (125). Using the intrinsic Knight shift for $YH_{1.92}$ and a value of $T_{1e}T$ = 269 sec K, a value of ρ = 1.0 was obtained. No corrections were made for susceptibility effects of the powdered sample. This value of ρ would indicate a suitable description by the free electron model. Norath and Fromhold (126) have reported values of ρ for ^{89}Y in Y metal (ρ = 1.26) and in YH_2 (ρ = 2.5). The variation of ρ among the elemental group III metals is very small. The ρ values of the metals are relatively close to the corresponding hydrides. The ρ values indicate the degree of electronic interactions at different physical positions in the metal hydride. However, the full meaning of the comparison of ρ values obtained from the metal and proton in the metallic hydride is unclear.

CONCLUSIONS

NMR provides a sensitive probe to obtain information about electronic structure, molecular structure, and motion. Until the advent of multiple pulse techniques for homonuclear decoupling, this information for protons in randomly oriented solids was inferred from conventional relaxation studies and wideline absorption. However, homonuclear decoupling alone was able to provide shielding information on only the more chemically simple systems. The extension of the combined multiple pulse and sample spinning experiment to protons in randomly oriented samples now allows the measurement of shielding parameters in these materials. When the results from conventional measurements are combined with those from the high resolution experiments, NMR is able to provide a wealth of information.

For the hydrogen molybdenum bronze, the materials prepared by the hydrogen spillover technique and by the "wet" chemistry method are not identical. Two species of protons were found. At room temperature, there is evidence to suggest that the predominant species is not hydroxyl. In addition, the measurement of hydrogen diffusion in the bulk provided information about the rate limiting step for the formation of the bronze via hydrogen spillover.

The contributions of interactions other than the homonuclear dipolar interaction have been shown to be negligible for the

measurement of the hydrogen second moment in $YH_{1.92}$. The measurement of the proton Knight shift indicates a suitable description by the free electron model at the proton sites.

BIBLIOGRAPHY

1. Lauterbur, P. C. Nature 1973, 242, 190.

2. Mansfield, P.; Maudsley, A. A. Proc. 19th Congress Ampere 1976, 247.

3. Hinshaw, W. S.; Bottomsley, P. A.; Holland, G. N. Nature 1977, 270, 722.

4. Damadian, R.; Goldsmith, M.; Minskoff, L. Physiol. Chem. and Phys. 1977, 9, 97.

5. Derouane, E. G.; Fraissard, J.; Fripiat, J. J.; Stone, W. E. E. Catal. Rev. 1972, 7, 121.

6. Pfeifer, H. In "NMR Basic Principles and Progress"; Diehl, P.; Fluck, E.; Kosfeld, R., Ed.; Springer: Berlin, 1972; Vol. 7.

7. Bovey, F. A. "Nuclear Magnetic Resonance Spectroscopy"; Academic: New York, 1969.

8. Bovey, F. A. "High Resolution NMR of Macromolecules"; Academic: New York, 1972.

9. Slonim, I. Y.; Lyubimov, A. N. "The NMR of Polymers"; Plenum: New York, 1970.

10. Gerstein, B. C. In "Analytical Methods for Coal and Coal Products"; Karr, C., Ed,; Academic: New York, 1979; Vol. 3, p. 425.

11. Cotts, R. M. In "Topics in Applied Physics"; Alefeld, G.; Völkl, J., Ed.; Springer: Berlin, 1978; Vol. 28, p. 227.

12. Haeberlen, U. "High Resolution NMR in Solids. Selective Averaging"; Academic: New York, 1976.

13. Nehring, M. In "NMR Basic Principles and Progress"; Diehl, P.; Fluck, E.; Kosfeld, R., Ed.; Springer: Berlin, 1976; Vol. 11.

14. Cirillo, A. C. Ph.D. Dissertation, University of Wisconsin, Milwaukee, Wisc., 1979.

15. Bloch, F.; Hansen, W. W.; Packard, M. Phys. Rev. 1946, 70, 474.

16. Purcell, E. M.; Torrey, H. C.; Pound, R. V. Phys. Rev. 1946, 69, 37.

17. Bloembergen, N.; Purcell, E. M.; Pound, R. V. Phys. Rev. 1948, 73, 679.

18. Proctor, W. G.; Yu, F. C. Phys. Rev. 1951, 81, 20.

19. Ramsey, N. F. Phys. Rev. 1950, 78, 699.

20. Torrey, H. C. Phys. Rev. 1953, 92, 962.

21. Lowe, I. J.; Norberg, R. E. Phys. Rev. 1957, 107, 46.

22. Mehring, M.; Griffin, R. G.; Waugh, J. S. J. Chem. Phys. 1971, 55, 746.

23. Andrew, E. R.; Bradbury, A.; Eades, R. G. Arch. Sci. (Geneva) 1958, 11, 223.

24. Andrew, E. R.; Bradbury, A.; Eades, R. G. Nature 1958, 182, 1659.

25. Andrew, E. R. Arch. Sci. (Geneva) 1959, 12, 103.

26. Andrew, E. R.; Bradbury, A.; Eades, R. G. Nature 1959, 183, 1802.

27. Andrew, E. R.; Eades, R. G. Discuss. Faraday Soc. 1962, 34, 38.

28. Andrew, E. R.; Furnell, L. F. Mol. Phys. 1968, 15, 157.

29. Andrew, E. R; Wynn, V. T. Proc. Roy. Soc. 1966, 291A, 257.

30. Lowe, I. J. Phys. Rev. Letters 1959, 2, 285.

31. Abragam, A. "Principles of Nuclear Magnetism"; Clarendon: Oxford, 1961.

32. Andrew, E. R.; Eades, R. G. Proc. Roy. Soc. 1953, 216A, 398.

33. Andrew, E. R.; Hinshaw, W. S. Phys. Letters 1973, 43A, 113.

34. Ostroff, E. D.; Waugh, J. S. Phys. Rev. Letters 1966, 16, 1097.

35. Haeberlen, U.; Waugh, J. S. Phys. Rev. 1968, 175, 453.

36. Waugh, J. S.; Wang, C. H.; Huber, L. M.; Vold, R. L. J. Chem. Phys. 1968, 48, 662.

37. Waugh, J. S.; Huber, L. M.; Haeberlen, U. Phys. Rev. Letters 1968, 20, 180.

38. Haeberlen, U.; Ellet, Jr., J. D.; Waugh, J. S. J. Chem. Phys. 1971, 55, 53.

39. Evans, W. A. B. Ann. Phys. (New York) 1968, 48, 72.

40. Rhim, W.-K.; Elleman, D. D.; Vaughan, R. W. J. Chem. Phys. 1973, 58, 1772.

41. Rhim, W.-K.; Elleman, D. D.; Vaughan, R. W. J. Chem. Phys. 1973, 59, 3740.

42. Rhim, W.-K.; Elleman, D. D.; Schreiber, L. B.; Vaughan, R. W. J. Chem. Phys. 1974, 60, 4595.

43. Burum, D. P.; Rhim, W.-K. J. Chem. Phys. 1979, 71, 944.

44. Mansfield, P. J. Phys. C 1971, 4, 1444.

45. Mansfield, P.; Orchard, M. J.; Stalker, D. C.; Richards, K. H. B. Phys. Rev. B 1973, 7, 90.

46. Dybowski, C. R.; Vaughan, R. W. Macromolecules 1975, 8, 50.

47. Lau, K. F.; Vaughan, R. W.; Satterthwaite, C. B. Phys. Rev. B 1977, 15, 2449.

48. Dybowski, C.; Pembleton, R. G. J. Chem. Phys. 1979, 70, 1962.

49. Carr, H. Y.; Purcell, E. M. Phys. Rev. 1954, 94, 630.

50. Pines, A.; Gibby, M. G.; Waugh, J. S. J. Chem. Phys. 1972, 56, 1176.

51. Pines, A.; Gibby, M. G.; Waugh, J. S. J. Chem. Phys. 1973, 59, 569.

52. Schaefer, J.; Stejskal, E. O.; Buchdahl, R. Macromolecules 1975, 8, 291.

53. Schaefer, J.; Stejskal, E. O. J. Am. Chem. Soc. 1976, 98, 1031.

54. Schaefer, J.; Stejskal, E. O.; Buchdahl, R. Macromolecules 1977, 10, 384.

55. Gerstein, B. C.; Pembleton, R. G.; Wilson, R. C.; Ryan, L. M. J. Chem. Phys. 1977, 66, 361.

56. Lippma, E.; Alla, M.; Tuherm, T. Proc. 19th Congress Ampere 1976, 113.

57. Stejskal, E. O.; Schaefer, J.; McKay, R. A. J. Mag. Res. 1977, 25, 569.

58. Abdo, S.; LoJacano, M.; Clarkson, R. B.; Hall, W. Keith J. Catal. 1975, 36, 330.

59. Cirillo, A.; Fripiat, J. J. J. Physique 1978, 39, 247.

60. Cirillo, A.; Ryan, L. M.; Gerstein, B. C.; Fripiat, J. J. J. Chem. Phys., in press.

61. Tinet, D.; Canesson, P.; Estrade, H.; Fripiat, J. J. J. Phys. and Chem. Solids, submitted.

62. Tinet, D.; Fripiat, J. J. J. Chemie Physique, in press.

63. Birtill, J. J.; Dickens, P. G. Mater. Res. Bull. 1978, 13, 311.

64. Dickens, P. G.; Birtill, J. J.; Wright, C. J. J. Solid State Chem. 1979, 28, 185.

65. Birtill, J. J.; Dickens, P. G. J. Solid State Chem. 1979, 29, 367.

66. Slade, R. C. T.; Halstead, R. K.; Dickens, P. G. J. Solid State Chem., in press.

67. Taylor, R. E.; Silva Crawford, M. M.; Gerstein, B. C. J. Catal. 1980, 62, 401.

68. Suchert, J. P. "Crystal Chemistry and Semiconduction in Transition Metal Binary Oxides"; Academic: New York, 1971.

69. Andersson, G.; Magnéli, A. Acta Chem. Scand. 1950, 4, 793.

70. Sermon, P. A.; Bond, G. C. Farad. Trans. 1976, 72, 730.

71. Glemser, O.; Lutz, G. Z. Anorg. Allg. Chem. 1951, 264, 17.

72. Sinfelt, J. H.; Lucchesi, P. J. J. Am. Chem. Soc. 1963, 85, 3365.

73. Sermon, P. A.; Bond, G. C. Catal. Rev. 1973, 8, 211.

74. Carcosset, H.; Delmon, B. Ind. Chim. Belg. 1973, 38, 481.

75. Sastri, M. V. C. Chem. Ind. Dev. 1975, 9, 52.

76. Fujimoto, K.; Asaoka, S. Sekiyu Gakkai 1976, 19, 837.

77. Vannice, M. A.; Boudart, M.; Fripiat, J. J. J. Catal. 1970, 17, 359.

78. Norberg. R. E. Phys. Rev. 1952, 86, 745.

79. Anderson, D. L.; Barnes, R. G.; Nelson, S. O.; Torgeson, D. R. Phys. Letters 1979, 74A, 427.

80. Anderson, D. L.; Barnes, R. G.; Peterson, D. T.; Torgeson, D. R. Phys. Rev. B, submitted.

81. Anderson, D. L.; Barnes, R. G.; Hwang, T. Y.; Peterson, D. T.; Torgeson, D. R. J. Less Common Metals, submitted.

82. Mueller, W. M.; Blackledge, J. P.; Libowitz, G. G. "Metal Hydrides"; Academic: New York, 1968.

83. Khatamian, D.; Kamitakahara, W. A.; Barnes, R. G.; Peterson, D. T. Phys. Rev. B, in press.

84. Venturini, E. L.; Richards, P. M. Phys. Letters, in press.

85. Khodosov, E. F.; Shepilov, N. A. Phys. Stat. Sol. 1972, 49, 83K.

86. Korringa, J. Physica 1950, 16, 601.

87. Hahn, E. L. Phys. Rev. 1950, 80, 580.

88. Stejskal, E. O.; Tanner, J. E. J. Chem. Phys. 1365, 42, 288.

89. Evans, W. A. B.; Powles, J. G. Proc. Phys. Soc. (London) 1967, 92, 1046.

90. Magnus, W. Commun. Pure Appl. Math. 1954, 7, 649.

91. Pembleton, R. G. Ph.D. Disseration, Iowa State University, Ames, Iowa, 1978.

92. Ellet, J. D.; Gibby, M. G.; Haeberlen, U.; Huber, L. M.; Mehring, M.; Pines, A.; Waugh, J. S. Adv. Mag. Res. 1971, 5, 117.

93. Adduci, D. J.; Gerstein, B. C. Rev. Sci. Instrum. 1979, 50, 1403.

94. Pembleton, R. G.; Ryan, L. M.; Gerstein, B. C. Rev. Sci. Instrum. 1977, 48, 1286.

95. Taylor, R. E.; Tindall, P.; Ryan, L. M.; Gerstein, B. C., in preparation.

96. Gerstein, B. C.; Chow, C.; Pembleton, R. G.; Wilson, R. C. J. Phys. Chem. 1977, 81, 565.

97. Webster, D. S.; Marshen, K. H. Rev. Sci. Instrum. 1974, 45, 1232.

98. Tomlinson, D. T. Mol. Phys. 1972, 25, 735.

99. Preissing, G.; Noack, F.; Kosfeld, R.; Gross, D. Z. Physik 1971, 246, 84.

100. James, T. L.; McDonald, G. G. J. Mag. Res. 1973, 11, 58.

101. Kida, J.; Uedaira, H. J. Mag. Res. 1977, 27, 253.

102. Gerstein, B. C.; Pembleton, R. G. Anal. Chem. 1977, 49, 75.

103. Ryan, L. M.; Taylor, R. E.; Paff, A. J.; Gerstein, B. C. J. Chem. Phys. 1980, 72, 508.

104. Anca, R.; Carrera, S. M.; Bianco, S. G. Acta Crystaliogr. 1967, 23, 1010.

105. Taylor, R. E.; Pembleton, R. G.; Ryan, L. M.; Gerstein, B. C. J. Chem. Phys. 1979, 71, 4541.

106. Haeberlen, U.; Kohlschüter, U. Chem. Phys. 1973, 2, 76.

107. Raber, H.; Brünger, G.; Mehring, M. Chem. Phys. Letters 1973, 23, 400.

108. Suwelack, D.; Becker, J.; Mehring, M. Solid State Commun. 1977, 22, 597.

109. Luly, M. H. "APES - A Fortran Program to Analyze Photoelectron Spectra", #IS-4694, Ames Laboratory, U. S. D. O. E., Ames, Iowa 50011.

110. Kim, K. S.; Baitinger, W. E.; Amy, J. W.; Winograd, N. J. Elect. Spec. and Rel. Phen. 1974, 5, 357.

111. Cimino, A.; DeAngelis, B. A. J. Catal. 1975, 36, 11.

112. Kapura, S.; Müller, E. W. Surf. Sci. 1977, 71, 944.

113. Ryan, L. M.; Wilson, R. C.; Gerstein, B. C. Chem. Phys. Letters 1977, 52, 341.

114. Burum, D. P.; Rhim, W.-K. J. Chem. Phys. 1979, 70, 3553.

115. Schreiber, D. S. Solid State Comm. 1974, 14, 177.

116. Levy, R. B.; Boudart, M. J. J. Catal. 1974, 32, 304.

117. Bendt, P. J. Phys. Rev. 1958, 110, 85.

118. Schwarz, H. A. J. Phys. Chem. 1969, 73, 1928.

119. Touillaux, R.; Salvador, P.; Van Meerssche, C.; Fripiat, J. J. Israel J. Chem. 1968, 6, 337.

120. Schmidt, K. N.; Buck, W. L. Science 1966, 151, 70.

121. Anderson, D. L. M.S. Dissertation, Iowa State University, Ames, Iowa, 1979.

122. Harper, W. C.; Barnes, R. G. J. Mag. Res. 1976, 21, 507.

123. Barnes, R. G., Department of Physics, Iowa State University, private communication.

124. Schreiber, D. S. Phys. Rev. 1965, 137, A860.

125. Reid, R. V. Phys. Rev. A 1975, 11, 403.

126. Norath, A.; Fromhold, T. Phys. Letters 1967, 25A, 49.